Attitude Determination and Prediction of Spin-Stabilized Satellites

By L. C. THOMAS and J. O. CAPPELLARI

(Manuscript received February 17, 1964)

Techniques for both attitude determination and prediction for spin-stabilized satellites are developed. Their use is demonstrated using Telstar I and II satellite data. It is shown that an inclined dipole model of the earth's magnetic field and the method of averaging the gravitational and magnetic torques over each anomalistic period of the satellite permits attitude predictions to within a few tenths of a degree of determined values in most instances. In those few cases where departures are above one degree, explanations are presented to show the reason for such discrepancies.

The usefulness of combining optical flash and solar sensor data for attitude determination and their inherent accuracy are demonstrated. Optical flash data can provide loci with a resolution of 0.1°. Solar sensor loci are resolved to within 1°.

All techniques described have been consolidated into working computer programs which follow closely the mathematical analysis presented. A number of important supporting calculations such as the solar position, sidereal time, orbit updating, etc. are also developed. Because of the complexities of the mean torque and gyroscopic equations, the precessional techniques presented are most useful in computer embodiments.

Table of Contents

I. INTRODUCTION

To maintain a defined attitude in space, the Telstar I and II satellites were spin stabilized. By this method of passive attitude control, a satellite is rotated about an axis of symmetry and consequently exhibits the characteristics of a gyroscope. In the absence of disturbing torques, the satellite's spin axis maintains its spatial orientation fixed with respect to an inertial reference frame throughout its orbit. For the Telstar I and II satellites, this is desirable because of certain required attitude constraints. First of all, the satellite communication antenna is not omnidirectional. More energy is radiated along the equator of the satellite than along its spin poles, as shown by the antenna pattern of Fig. 1. This fact dictates an attitude for which the line of sight from

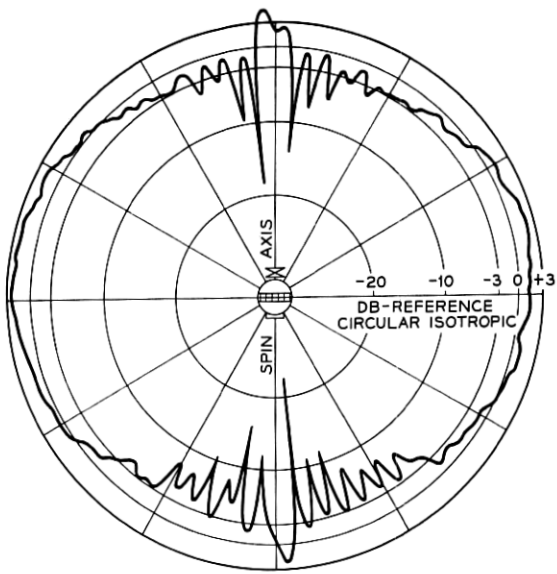

Fig. 1 — Antenna pattern at 4170 mc.

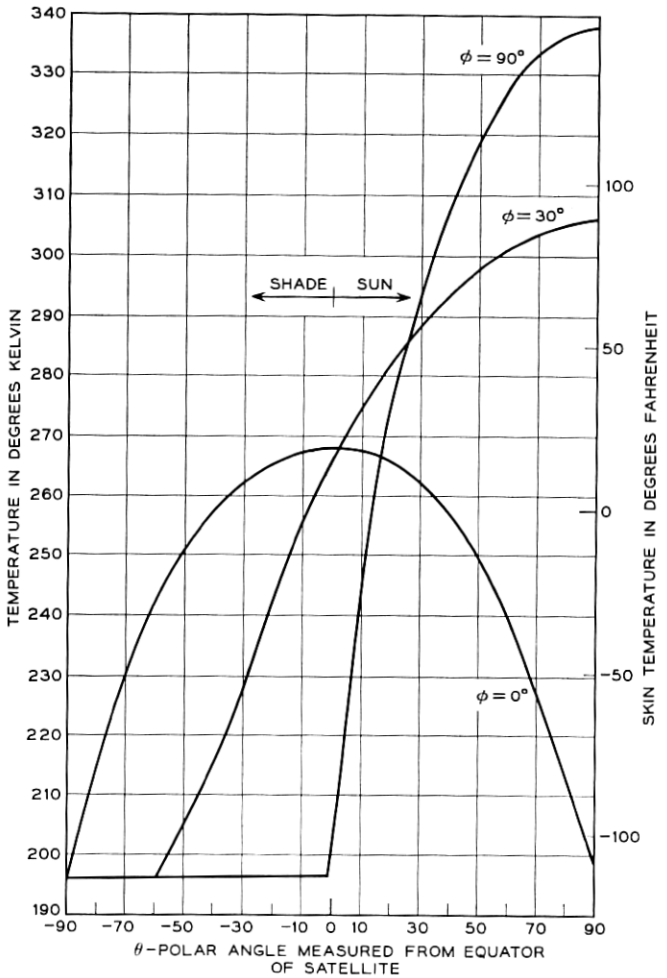

Fig. 2 — Skin temperature distribution vs polar angle.

a ground station to the satellite avoids its poles. The second attitude constraint involves temperature considerations. A good degree of temperature control is obtained by orienting the spin axis so that it is nearly perpendicular to the satellite-sun line. In this manner, temperature balance is maintained by the satellite's spin as indicated in Fig. 2. Here, φ is the solar offset angle, defined as the angular departure of the spin axis from perpendicularity with the satellite-sun line. Solar offsets of about 15° result in temperature deviations of about 150° (see Fig. 2) and are tolerable.

An ideal orientation from a communications standpoint would be to have the spin axis nearly parallel to the earth's surface as it passes over any ground station. A spin axis perpendicular to the orbital plane would accomplish this, but would produce a maximum axis tilt toward the sun equal to the sum of the orbital inclination and the earth's $23\frac{1}{2}°$ tilt with respect to the plane of the ecliptic (see Fig. 3). Under these conditions the spin axis of the first Telstar satellite would have a maximum solar tilt of 68°. This exceeds the 15° tilt limit dictated by temperature

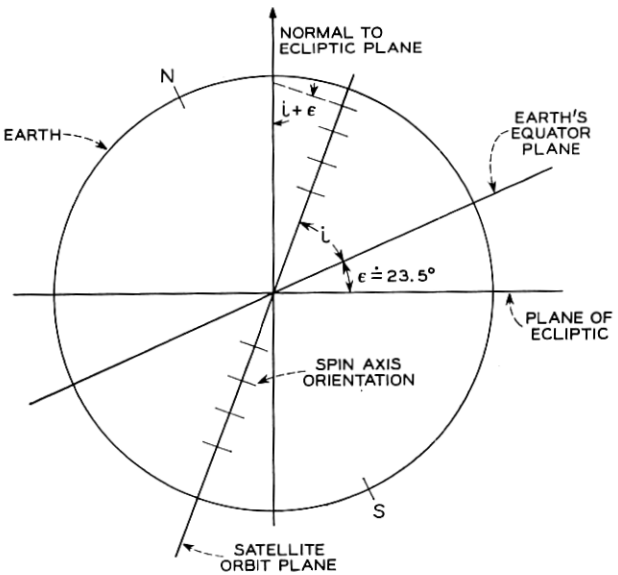

Fig. 3 — Geometry of spin axis perpendicular to orbit plane.

balance. On the other hand, if the spin axis is made perpendicular to the ecliptic plane (which automatically insures its perpendicularity to the sun), the axis tilt with respect to the line of sight from any ground station over which it may be passing will range from 90° to 90° minus the sum of the orbit inclination and ecliptic obliquity or 22° (see Fig. 4).* From a communications standpoint this is tolerable, since nulls in the antenna pattern are major only within about 15° of the spin

* With this orientation, stations south of the satellite's instantaneous earth latitude would experience angles less than 22°, such as station B of Fig. 4. The major ground stations for Telstar I and II, however, are all at latitudes above 43°. Since the inclinations of the Telstar I and II satellites are 45° and 42.7° respectively, these stations are almost always north of the satellite.

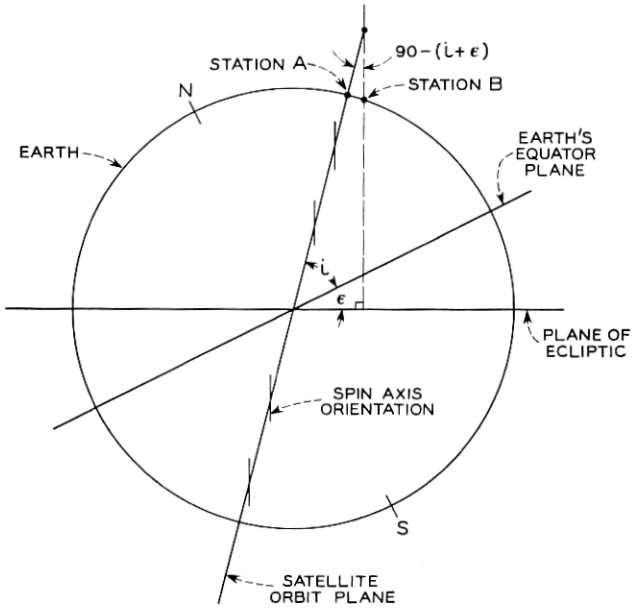

Fig. 4 — Geometry of spin axis perpendicular to ecliptic.

poles (see Fig. 1). Rising and setting satellites may experience a greater tilt to the ground station line of sight, but this is unavoidable.

Because of these considerations, the Telstar I and II satellites were launched with their spin axes as nearly perpendicular to the ecliptic as the powered flight trajectory of the Thor-Delta launch vehicle would permit and still meet certain orbital requirements, such as inclination, apogee height, and perigee height.[1] The predicted attitudes of these satellites at orbit injection are calculated from telemetry data from the first and second rocket stages. Table I lists these attitudes as the right ascension and declination direction of the north pole of the satellite.

TABLE I — ATTITUDE OF THE TELSTAR I AND II SATELLITES AT INJECTION, DETERMINED FROM POWERED FLIGHT DATA

Satellite	Initial Attitude	
	Right Ascension	Declination
Telstar I	83.73°	−66.80°
Telstar II	82.23°	−57.31°

The north pole is defined here as the direction of advance of a right-handed screw turning in the direction of the satellite's spin. It also happens to be the spin pole which carries a helical telemetry antenna.

The initial attitudes of the Telstar I and II satellites are changed by gyroscopic precession. This motion of spin-stabilized satellites is chiefly produced by both magnetic and gravitational torques. The former is a result of interaction between residual and eddy-current-produced magnetic fields of the satellite and the earth's magnetic field. The latter is produced by differential gravitational forces acting across the body of the satellite. In the present cases, the magnetic torques are several orders of magnitude in excess of the gravitational torques.

It is necessary to predict precession to allow proper scheduling and planning for satellite use, to resolve certain attitude determination ambiguities, and to sensibly plan alteration of satellite attitude in a prescribed manner when needed. (See Section V for a description of this technique.) It is the purpose of this paper to outline the methods of attitude determination and correction, to develop the precessional theory, and to show the application of these to the Telstar I and II satellites.

II. ATTITUDE DETERMINATION — GENERAL REMARKS

The attitude of the Telstar I satellite has been determined through the analysis of two sets of data: the time of optical flashes of sunlight from three mirrors attached to the surface of Telstar and the current produced by six on-board solar sensors located on the ends of three orthogonal axes.

The first of these sets of data in combination with the spatial position of the satellite, sun, and observer's position determines a locus of possible spin axis positions which would result in the observed flash. This locus describes a cone in space whose axis is the mirror normal. The six solar sensors are designed to determine the direction of the satellite-sun line with respect to a satellite frame of reference and thus to the spin axis. Knowing this angle, again there is defined a conical array of possible spatial spin axis directions. The intersection of the optical cone with this solar sensor cone should, therefore, determine two possible attitudes. A priori knowledge of the approximate attitude as provided by launch data and/or a succession of measurements and predictions over an interval of several days permits the determination of a unique spin axis direction in space.

In practice, the solar sensors present a few difficulties. First of all, the deduction of the sun's position from solar cell current entails inferring

a solar angle between each cell's normal and the sun's direction. Such a direction from each of three cells uniquely establishes this solar aspect.* Thus calibration curves relating electrical output to light intensity must be employed for each cell along with temperature corrections. While D. W. Hill[2] has prepared a computer program to take the drudgery out of this work, it remains difficult to calculate the solar angle for a cell if it is illuminated in a direction far from its normal. Moreover, the solar sensor data, which are reported every minute by telemetry, were found to be not always mutually consistent. Often, the solar direction calculated over 30 minutes from a succession of telemetry frames had a spread ranging from 1° to over 8°. A correlation between these deviations and the spatial position of the satellite exists which suggests a biasing of solar cell data, on occasion, by the earth's reflectivity.

To show the geometry of this situation, consider the satellite position shown in Fig. 5. Here one half of the satellite to the right of line AB is

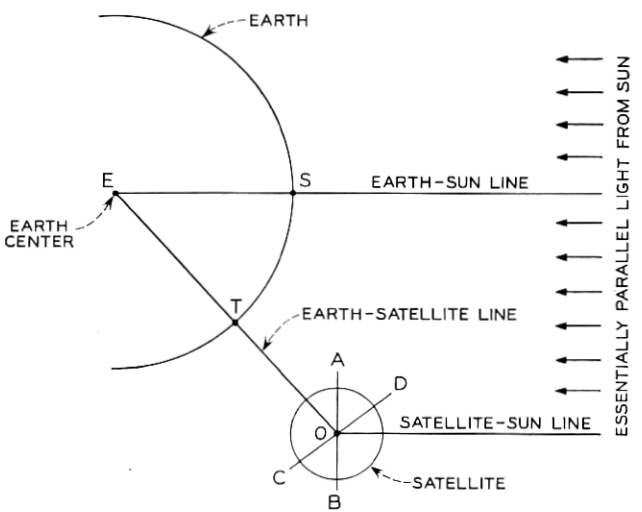

Fig. 5 — Satellite shadow geometry.

illuminated by the sun. At least one half, to the upper left of line CD, is illuminated by the earth in reflecting about 38 per cent† of the sun's total incident light. Thus a solar cell in region BOD would record only direct sunlight, one in region AOC would record only earthshine, and

* The solar aspect is the angle between the satellite's spin axis and the satellite-sun line.

† This is not the albedo but the earth's mean reflectivity or ratio of mean earth brightness measured at a spot along the earth-sun line relative to the brightness of a perfectly diffusing disk of the same size and at the same distance that the

one in region AOD would record both. There would be no light from either the sun or the earth in region COB. By the difference in solar illumination and earthshine, data from cells in regions BOD and AOC are easily separated and the latter disregarded. However, those cells in region AOD measure both sunlight and earthshine in an inseparable manner and therefore report erroneously the sun's position. If AOD is a large angle, the spin of the satellite will carry solar sensors into that region frequently and result in sizable variations in successive solar aspect determinations. Since AOD equals SET, as the subsatellite position (T) departs from the subsolar point (S), the solar cell data must be carefully interpreted to avoid false conclusions. Under these conditions, it would be wrong, for example, to simply calculate the mean of all solar aspect determinations over a succession of telemetry frames. This procedure, in general, would not yield a good estimate of the true aspect. A better technique would be to calculate the mean for only those solar aspect determinations in which all three cells entering into the determination exhibited current readings above those which could possibly be produced by either the earth's reflectivity or low angles of solar illumination. Operating in this fashion, the true solar aspect can be determined to within about 1°.

Since the maximum attitude resolution obtainable using optical flashes from the Telstar satellites is about 0.1°, it was decided to rely on these for attitude determinations insofar as possible. Two groups of flashes close together in time are needed for an attitude fix, however, and in cases where only a single one existed, the attitude was determined by a combination of mirror flashes and the solar sensor data previously described.

The optical reflections are characterized by a series of intermittent flashes provided by the spin of the Telstar satellites. The time midpoint of these flash series is determined by photoelectric equipment[3] at Bell Telephone Laboratories in Holmdel, N. J. The time of each flash series determines a conical locus of possible spin axis positions about the flashing mirror's normal. The tip of the spin axis vector, therefore, lies on a circle on the celestial sphere. One of the intersections of two such circles defines the attitude, provided the two corresponding flash series occur close enough together in time so that no appreciable precession occurs during the separation interval. Since the mirrors employed have their normals far removed from the spin axis (68° and 95°), it is

earth is from the given spot. Quite naturally a phase law applies which reduces the light reflected to points off the earth-sun line. Off-line brightness varies crudely as the ratio of observable illuminated area of the earth as seen from the point in question to the total observable illuminated area seen from a point on the earth-sun line.

always possible to select the valid locus intersection from past performance and attitude predictions.

III. ATTITUDE DETERMINATION — COMPUTATIONAL TECHNIQUE

A computational technique has been developed for the calculation of spin loci. It consists of four basic parts, which are:

(*i*) the determination of the right ascension and declination of the normal of the flashing mirror;

(*ii*) the determination of the right ascension and declination of the sun in the case of solar cell data;

(*iii*) the construction of a circular locus on the celestial sphere centered on the right ascension and declination of the mirror normal and having a radius of 68° or 95°, depending upon the mirror involved (in the case of solar aspect data from the sensors, the locus is centered on the right ascension and declination of the sun and has a radius equal to the measured solar aspect angle);

(*iv*) the plotting, by computer microfilm techniques, of these circles and others determined from additional flash series and solar aspect data to ascertain intersections and corresponding satellite attitudes.

3.1 *The Right Ascension and Declination of the Mirror Normal*

Consider the generalized mirror orientation shown in Fig. 6. Here, a ray from the sun strikes the mirror and is reflected toward a particular

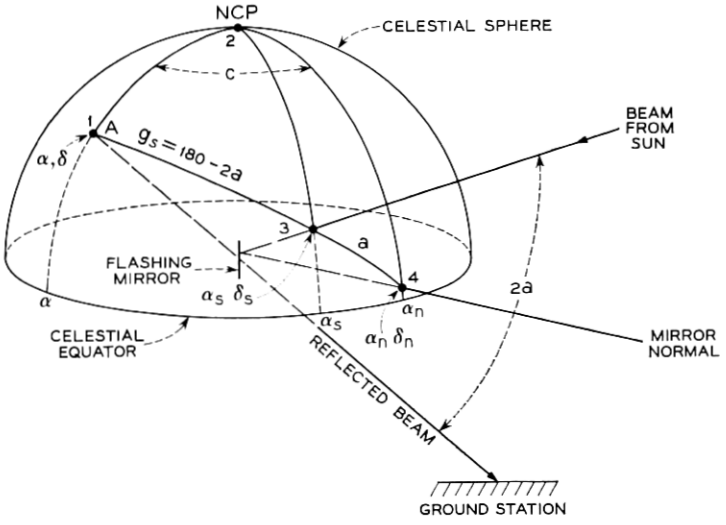

Fig. 6 — Geometry of mirror normal.

ground station. For this to be possible, the mirror normal must bisect the angle $2a$ and lie in the plane determined by the mirror-sun line and the mirror-ground station line.

Sketched around the mirror in Fig. 6 is the celestial sphere. On this sphere the solar direction, as seen from the mirror, is indicated by its right ascension, α_s, and its declination, δ_s. In like fashion, the direction of the satellite mirror as seen from the ground station is specified as α,δ and the direction of the mirror normal is $\alpha_n\delta_n$.

To determine α_n and δ_n, we begin by solving for arc g_s and A in the spherical triangle 1, 2, 3:

$$\cos g_s = \sin \delta \sin \delta_s + \cos \delta \cos \delta_s \cos (\alpha_s - \alpha) \tag{1}$$

$$\cos A = \frac{\sin \delta_s - \sin \delta \cos g_s}{\cos \delta \sin g_s} \tag{2}$$

where angles g_s and A may have values from 0° to 180°.

By triangle 1, 2, 4, one obtains the declination of the normal as

$$\delta_n = \sin^{-1} [\sin \delta \cos g_s + \cos \delta \sin g_s \cos A] \tag{3}$$

where δ_n may have values between ±90°.

Using the same triangle we may write

$$C = \sin^{-1} \left[\frac{\sin (g_s + a) \sin \delta_n}{\sin A} \right] \tag{4}$$

where

$$A = \frac{180 - g_s}{2}. \tag{5}$$

C may have values between 0° and 180°. Since α_n may either exceed α by C or be less by the same amount owing to the two possible orientations of triangle 1, 2, 4, we have

$$\alpha_n = \alpha + \text{SIGNF } (C,\alpha_s - \alpha) \tag{6}$$

where SIGNF, a common computer symbol, indicates that the algebraic sign to be affixed to C shall be determined by the quantity $\alpha_s - \alpha$.

Right ascension is measured eastward from the vernal equinox as a 0 reference through 360°, and if α_s and α should lie on opposite sides in this reference (C remaining less than 180°), (6) becomes

$$\alpha_n = \alpha + \text{SIGNF } (C,\alpha - \alpha_s). \tag{7}$$

Thus (6) is employed if $|\alpha_s - \alpha| - 180°$ is negative and (7) if otherwise.

3.2 *The Right Ascension and Declination of the Sun*

The apparent right ascension and declination of the sun at any specified time is computed from the mean orbital elements of the sun.[4] These may be expressed beginning with the true solar mean anomaly in degrees as

$$M_s = 358.47583 + 0.9856002670d' - 0.000150T^2 - 0.000003T^3$$

where

T = the time in Julian centuries of 36525 ephemeris days from January 0.5, 1900, ephemeris time[5]
d' = ephemeris days from same epoch.

We may express the above equation in a more useful form for the present calculations by changing the epoch to January 1.0, 1960 and writing an equivalent expression as

$$M_s \doteq 357.41283 + 0.985600267d$$

where

d = ephemeris days since the 1960 epoch
= mean solar days since 1960 epoch + 1 second for the years 1963, 1964, 1965.

One obtains the apparent mean solar anomaly, used in the present calculations to determine the apparent position of the sun, by antedating for the solar light transit time. For this reason d is increased by 0.005375 day, which is the light transit time at mean solar distance. Since the earth is about 3×10^6 miles closer to the sun in winter as compared to summer, this can produce an error in apparent solar position of about 2 seconds of arc.

The eccentricity of the earth's orbit is

$$e = 0.01675104 - 0.00004180T - 1.26 \times 10^{-7}T^2$$
$$= 0.01700254 \text{ on January 1.0, 1960.}$$

Also, the degrees of mean celestial longitude of the perigee of the sun's mean orbit about the earth as a reference is

$$L = 279.69668 + 0.9856473354d' + 0.000303T^2$$
$$= 282.25247 + 0.470684 \times 10^{-4}d.$$

Finally, the mean obliquity of the ecliptic in degrees is

$$\epsilon = 23.452294 - 0.0130125T - 1.64 \times 10^{-6}T^2 + 5.03 \times 10^{-7}T^3.$$

The apparent mean anomaly and eccentricity along with Kepler's equation permit the calculations of the apparent true anomaly of the sun by standard techniques.[6] This along with the apparent mean longitude of solar perigee and mean obliquity of the ecliptic allows a direct determination of the apparent right ascension and declination of the sun at any date by the simple geometry shown in Fig. 7.

The apparent right ascension and declination of the sun computed from its mean elements in this manner can depart from the tabular values (which include nutation) of *The American Ephemeris and Nautical Almanac* for the years 1962, 1963, and 1964 by about 5 seconds of arc as a maximum. This is well within the approximate 1° error of the measuring techniques for solar aspect as well as the 0.1° for the mirror technique.

3.3 *Construction of the Locus Circle*

As previously stated, the direction of the spin axis may be specified as a circle on the celestial sphere, centered on the right ascension and declination of the mirror normal. This locus may be generated by using the spherical triangle shown in Fig. 8. Here the dotted curve indicates the attitude locus of all possible positions of the spin axis. Let $\alpha_l\delta_l$ be any point on this circle making a fixed arc F with α_n , δ_n . In the case of either the Telstar I or II satellite, F will equal 68° or 95°, the angles

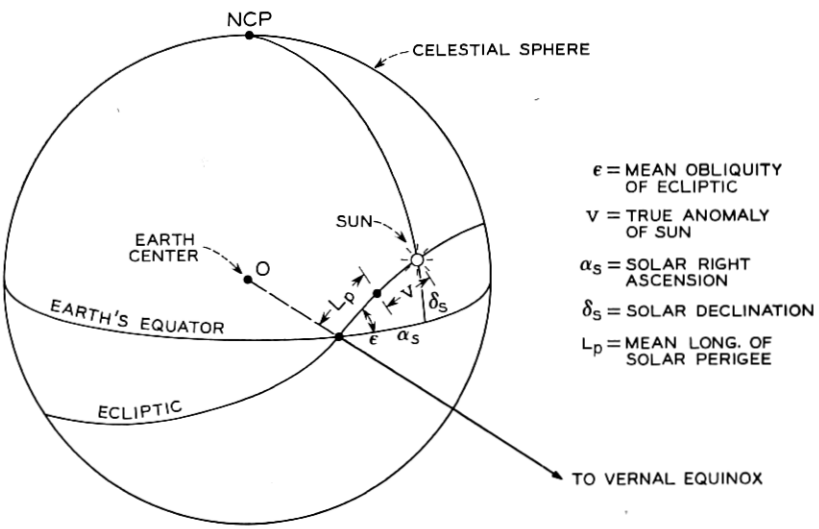

Fig. 7 — Geometry of the sun's position.

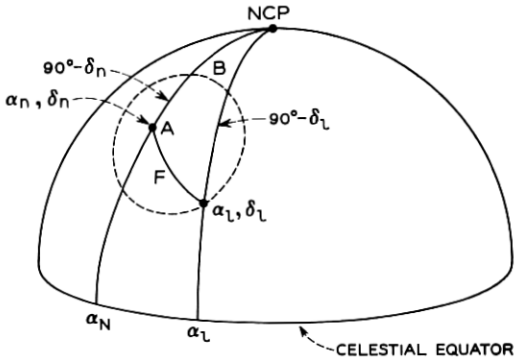

Fig. 8 — The attitude locus.

the mirror normals make with the spin axis. From Fig. 8,

$$\delta_l = \sin^{-1} [\sin \delta_n \cos F + \cos \delta_n \sin F \cos A] \tag{8}$$

where

A = a running variable which takes on values from 0 to 360° to generate the locus

δ_l = declination of a locus point which ranges from −90° to +90°, in general.

Also

$$\sin B = \frac{\sin F \sin A}{\cos \delta_l} \tag{9}$$

$$\cos B = \frac{(\cos F - \sin \delta_n) \sin \delta_l}{\cos \delta_n \cos \delta_l} \tag{9a}$$

$$B = \tan^{-1} \frac{\sin B}{\cos B} \tag{10}$$

and

$$\alpha_l = \alpha_n + B. \tag{10a}$$

In general, B may range from 0° to 360°. All quadrant ambiguities presented by (10) are resolved by noting the algebraic signs of (9) and (9a).

If there is a time uncertainty in measuring the midpoint of a flash series, this will result in more than one possible mirror normal, $\alpha_n \delta_n$, and hence a number of attitude loci, since the satellite and sun will occupy successive positions along their paths within the time error.

If during a single sky trajectory a ground station records two separate flash series (or a single series plus solar aspect data), each will generate a circular locus. The intersections of these loci determine attitude with an ambiguity of two. That is, there are two intersections and therefore two possible satellite attitudes which satisfy the two flash series. A priori knowledge of the attitude from previous measurements or initially from launch parameters together with some knowledge of the expected precession will permit selecting the proper intersection. Knowledge of expected precession is also needed to determine whether or not the flash series are close enough together in time to neglect incremental precession during the time between the series. Such precession can alter the position of the loci intersections.

Fig. 9 shows an example of the attitude determination of the Telstar II satellite for passes 135, 136, 199, 272, and 472. Solid lines indicate attitude loci determined from mirror flashes. The line of zeros is typical of those determined by solar sensor data. Two attitude determinations are shown by intersections on passes 135, 136, and on pass 272.

IV. ATTITUDE PREDICTION

Acting upon an orbiting spin-stabilized satellite to produce precession are certain disturbing torques. Those to be considered here are gravitational and magnetic torques. In the case of the Telstar I and II satellites, these are dominant over atmospheric drag torques, solar radiation torques, electrostatic torques, and others.

4.1 *Assumptions for Gravity Torque Calculations*

Differential gravity forces acting across the body of the satellite can produce torques which tend to rotate the body. These forces exist simply because the strength of the earth's gravity field is a function of the distance from earth. A body of finite size must, therefore, experience such torques.

For the purpose of calculating the mean gravity torques, the earth is assumed spherical with its radius equal to the equatorial radius. For the Telstar satellites, gravity torques are at least an order of magnitude less than magnetic torques, and therefore neglecting the earth's oblateness produces at worst only a second-order error.

It is also assumed that the moments of inertia of the satellites about all axes perpendicular to the spin axis and passing through the mass center are equal. The orbit is assumed elliptical and Keplerian, since the earth's figure produces but second-order effects over a single satel-

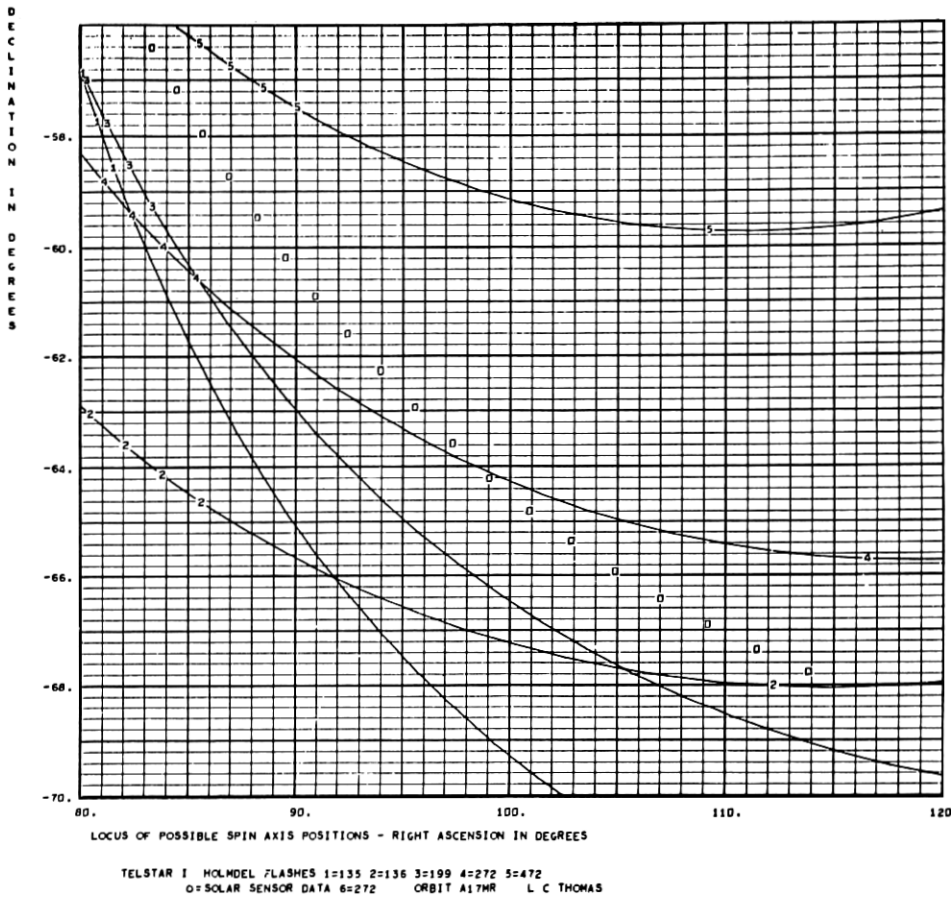

Fig. 9 — Computer plot of mirror and solar loci.

lite period. The orbit, however, for each succession of calculations will be updated using mean orbital elements, which include all secular perturbations, to produce the Keplerian orbit of the best fit at the beginning of each calculation.

4.2 *Assumptions for Magnetic Torque Calculations*

In order to construct a mathematical model which on one hand reasonably well represents the physics of the situation, but on the other hand does not, by its complexity, produce numerical equations costly to compute, the following simplifying assumptions are made:

(*i*) The magnetic field of the earth is represented by a dipole centered at the earth's center and inclined β degrees (equal 11.4°) to the earth's spin axis.[7,8]

(*ii*) Mass symmetry about the satellite's spin axis exists, as in Section 4.1.

(*iii*) The effects of magnetic moments transverse to the spin axis are either negligible or average out due to the satellite's spin.

(*iv*) For the calculation of mean or net magnetic torques over an orbital period, a Keplerian orbit is assumed as in Section 4.1.

4.3 *Assumptions for Gyroscopic Equations of Motion*

It will be useful in simplifying the gyroscopic equations of motion (see Section 4.7) to assume that the satellite angular momentum vector coincides with the spin axis and equals the spin rate times the moment of inertia about the spin axis. This is the same as assuming the entire angular momentum of the satellite is the result of its spin alone, and neglects that small amount provided by the precession of the spin axis itself. Precessional dampers[9] are provided on the Telstar satellites to prevent coning or rapid changes in attitude at rates comparable to the spin rate. This, more than ever, makes the assumption quite reasonable.

4.4 *Coordinate Systems*

It will be convenient to establish certain useful coordinate systems and their interrelationships prior to the torque calculations. These will be defined and related by Euler-type axis rotations expressed by matrices. All coordinate systems are rectangular and right-handed in the conventional sense such that the rotation of an X axis into a Y axis determines the positive direction of a Z axis as the direction of progress of a right-handed screw. Each system will be named, described, and interrelated in that order.

4.4.1 *The Earth-Centered Inertial System (IS)*

In this system, the three mutually perpendicular X, Y, and Z axes have their common origin at the earth's center. X contains the vernal equinox and increases positively from the earth's center in its direction. Y is perpendicular to X in the earth's equatorial plane. Z contains the earth's spin axis and increases positively toward the north celestial pole. This is the basic system to which others will be referred.

4.4.2 *Rigid-Body Systems*

Two rigid-body systems will be used. Both have their origin at the satellite mass center. The first of these is to be known as the SANOR or satellite nonrotating system. In this system, the z axis defines the satellite's spin axis, being positive in the direction of advance of a right-hand screw spinning with the satellite. The x axis is in the satellite

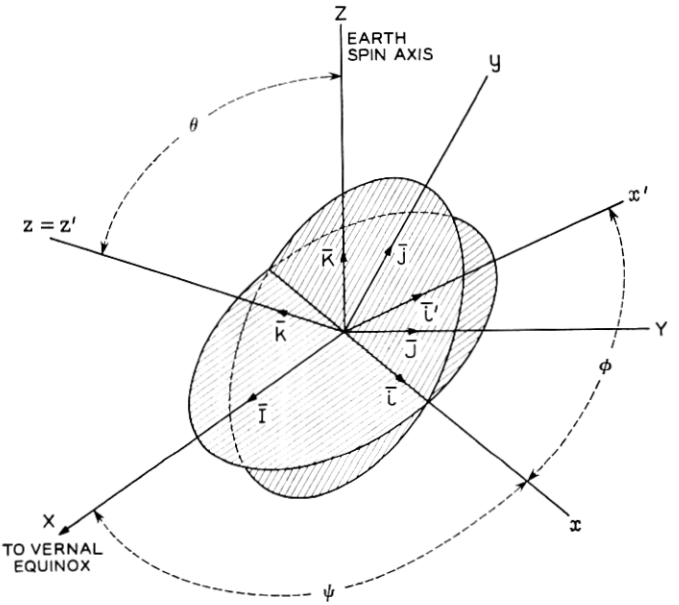

Fig. 10 — The IS, SANOR and SAR systems.

equatorial plane, ψ degrees rotated from X (see Fig. 10) about Z. This axis defines the xy-XY plane intersection. The y axis is in the satellite equatorial plane orthogonal to x. At this point, we note that the rotational equations of motion for the satellite will be developed in this SANOR system.

The SAR or satellite rotating system, as its name implies, differs from the SANOR system in that it rotates with the satellite. It has axes x', y', z', where z' coincides with z, and x' and y' are defined as being rotated φ degrees from x and y respectively about z.

To relate the SANOR and SAR systems to IS, we proceed as follows (refer to Fig. 10). The ψ rotation about Z yields the following matrix

$$D = \begin{vmatrix} \cos\psi & \sin\psi & 0 \\ -\sin\psi & \cos\psi & 0 \\ 0 & 0 & 1 \end{vmatrix}. \tag{11}$$

The θ rotation about x yields

$$C = \begin{vmatrix} 1 & 0 & 0 \\ 0 & \cos\theta & \sin\theta \\ 0 & -\sin\theta & \cos\theta \end{vmatrix}. \tag{12}$$

The φ rotation about z gives

$$B = \begin{vmatrix} \cos\varphi & \sin\varphi & 0 \\ -\sin\varphi & \cos\varphi & 0 \\ 0 & 0 & 1 \end{vmatrix}. \tag{13}$$

To transfer points in the IS to points in the SANOR system, we have

$$\begin{vmatrix} x \\ y \\ z \end{vmatrix} = (CD) \begin{vmatrix} X \\ Y \\ Z \end{vmatrix} \tag{14}$$

or, just to shorten the notation

$$x = (CD)X \tag{15}$$

where

$$(CD) = \text{multiplication of the } C \text{ and } D \text{ matrices.}$$

In like fashion

$$\mathrm{a}' = (BCD)X \tag{16}$$

$$= AX \tag{17}$$

where

$$A \equiv (BCD) = \text{multiplication of the } B, C, D \text{ matrices.}$$

Carrying out this multiplication, we may express A as the following

$$A = \begin{vmatrix} \cos\psi\cos\varphi & \cos\varphi\sin\psi & \sin\varphi\sin\theta \\ \quad -\cos\theta\sin\varphi\sin\psi & \quad +\cos\theta\cos\psi\sin\varphi & \\ -\sin\varphi\cos\psi & -\sin\varphi\sin\psi & \cos\varphi\sin\theta \\ \quad -\cos\theta\sin\psi\cos\varphi & \quad +\cos\theta\cos\psi\cos\varphi & \\ \quad \sin\theta\sin\psi & \quad -\sin\theta\cos\psi & \cos\theta \end{vmatrix}. \quad (18)$$

The matrix CD may be obtained from A by letting $\varphi = 0$,

$$(CD) = \begin{vmatrix} \cos\psi & \sin\psi & 0 \\ -\sin\psi\cos\theta & \cos\psi\cos\theta & \sin\theta \\ \sin\psi\sin\theta & -\cos\psi\sin\theta & \cos\theta \end{vmatrix}. \quad (19)$$

Quite obviously the inverse operations apply by taking the transposes of the matrices. Indicating a transposed matrix by the symbol $\sim$, we have

$$X = (\tilde{D}\tilde{C})x \quad (20)$$

and

$$X = \tilde{A}x'. \quad (21)$$

4.4.3 *Orbital Coordinate Systems*

Let an orbit defining system (ORDEF) be described along the lines shown in Fig. 11. Here x_g is the intersection of the orbit plane and the earth's equator plane with $+x_g$ drawn toward the ascending node of the orbit from the earth's center. Axis z_g is normal to the orbit plane, positive in a direction a right-handed screw along oz_g would advance if turned in the direction of the satellite's orbital motion. Axis y_g completes a right-handed system by being mutually perpendicular to x_g and z_g.

The satellite defining system (SADEF) has its z_s axis collinear with z_g, but x_s passes through the instantaneous satellite position, ω degrees from x_g. Axis x_s therefore will be referred to as the local vertical of the satellite.

The ORDEF and SADEF systems are related to the inertial system (IS) in a manner strictly analogous to the SANOR and the SAR matrices described in the previous section. The only change in the matrices is that

$$\Omega \text{ replaces } \psi$$

$$i \text{ replaces } \theta$$

$$\omega \text{ replaces } \varphi.$$

Thus we may write

$$x_g = (CD)_i X \tag{22}$$

$$X = (\tilde{D}\tilde{C})_i x_g \tag{23}$$

$$x_s = A_i X \tag{24}$$

$$X = \tilde{A}_i x_s \tag{25}$$

where the subscript i indicates the Ω, i, ω substitution.

4.4.4 *Magnetic Coordinate System*

A magnetic coordinate system (MAG) based on an inclined dipole model of the earth's magnetic field is constructed as follows. Let axis x_m define the intersection of the geomagnetic equatorial plane with the earth's geographical equatorial plane, positive toward the ascending node of the geomagnetic equator ($\eta°$ from X, see Fig. 12). Axis z_m is

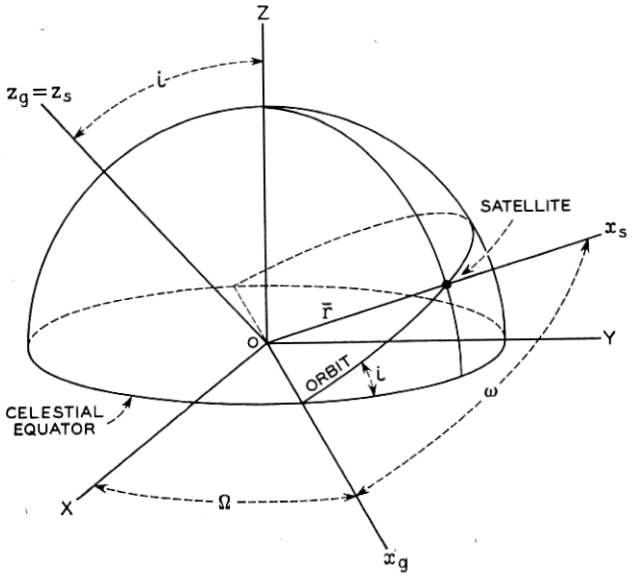

Fig. 11 — The ORDEF and SADEF coordinate systems.

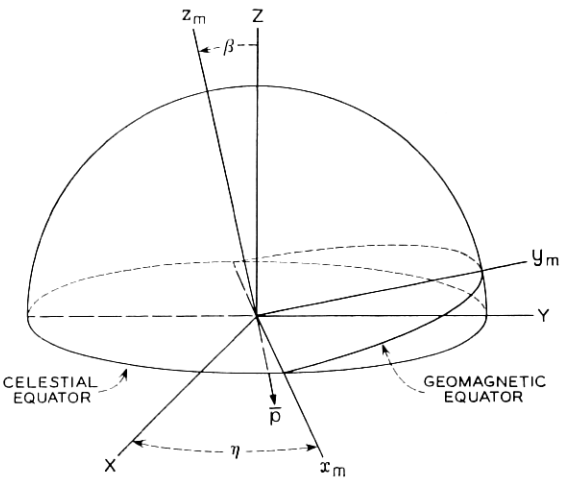

Fig. 12 — The geomagnetic coordinate system.

normal to the geomagnetic equator plane, positive toward the north geographical hemisphere, and $\beta°$ from Z. Here β is simply the magnetic dipole inclination to the earth's spin axis. Axis y_m is in the geomagnetic equatorial plane orthogonal to x_m.

Transformations from the MAG system into the IS system proceed as in (15) thru (20) with

$$\eta \text{ replacing } \psi$$

$$\beta \text{ replacing } \theta$$

in the matrices, so that

$$x_m = (CD)_\eta X \tag{26}$$

and

$$X = (\tilde{D}\tilde{C})_\eta x_m . \tag{27}$$

where the subscript η on the matrices indicates the above substitutions.

Fig. 13 shows the orientation of the earth-centered inclined dipole which produces a field of best fit[7,8] to a field based on all observations of field vectors made anywhere over the earth's surface. The anomalies, or differences between the actual and dipole field, decrease more rapidly with increasing heights above the earth's surface than does the dipole field itself, making the fit better and better as altitude increases.

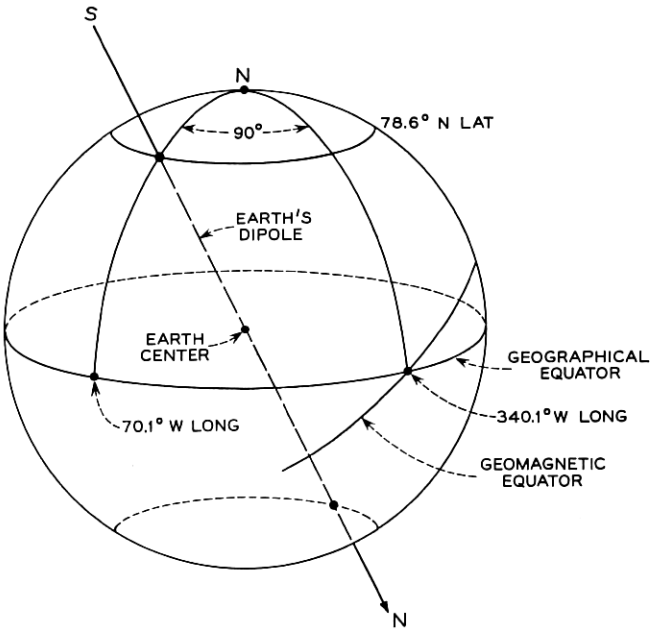

Fig. 13 — The earth-centered inclined dipole.

4.5 *The Mean Gravity Torque*

If the potential energy of an orbiting satellite is expanded about its center of mass in a Taylor series and differentiated with respect to the angles giving its orientation with respect to the IS coordinate system, the instantaneous gravitational torque acting on the satellite may be expressed as[10]

$$\mathbf{T}_g = 3\mu^2(I_3 - I)(\mathbf{i}_s \cdot \mathbf{k})(\mathbf{i}_s \times \mathbf{k}) \tag{28}$$

where

$$\mu^2 = GM/r^3 \tag{29}$$

GM = universal gravitational constant $\times$ the mass of the earth
r = geocentric distance of satellite
I_3 = moment of inertia about satellite's spin axis, z
I = moment of inertia transverse to z (assuming all transverse moments to be equal, i.e., $I_x = I_y$)
$\mathbf{k}$ = unit vector along satellite spin axis, z (more generally the

vector along the axis of cylindrical mass symmetry, which is the spin axis by assumptions in Section 4.1).

To determine the mean gravity torque, $\mathbf{T}_g$ will be integrated over a nodal period (T_n) assuming no precession during that period; i.e., the SANOR system stays fixed with respect to IS during the integration. Then

$$(\mathbf{T}_g)_{\text{mean}} = \frac{1}{T_n}\int_0^{T_n} 3\mu^2(I_3 - I_1)(\mathbf{i}_s\cdot\mathbf{k})(\mathbf{i}_s \times \mathbf{k})\, dt. \tag{30}$$

By interchanging the order of the dot product and taking $\mathbf{k}$ constant,

$$(\mathbf{T}_g)_{\text{mean}} = \frac{3GM(\Delta I)}{T_n}\left[\mathbf{k}\cdot\left\{\int_0^{T_n}\frac{\mathbf{i}_s\mathbf{i}_s}{r^3}\, dt\right\} \times \mathbf{k}\right]. \tag{31}$$

If a pure Keplerian orbit[6] is assumed, we have

$$r = \frac{a(1 - e^2)}{1 + e\cos(\omega - P)} \tag{32}$$

$$r^2\dot{\omega} = \frac{2\pi a^2(1 - e^2)^{\frac{1}{2}}}{T_n} \tag{33}$$

$$GM = \frac{4\pi^2 a^3}{T_n^2} \tag{34}$$

where

r = radius vector from the focus of the elliptical orbit to the satellite
a = semimajor axis of ellipse
e = eccentricity of the ellipse
P = argument of perigee
ω = argument of the satellite.

Hence the integral becomes

$$\int_0^{T_n}\frac{\mathbf{i}_s\mathbf{i}_s}{r^3}\, dt = \int_0^{\omega=2\pi}\frac{\mathbf{i}_s\mathbf{i}_s}{r^3\dot{\omega}}\, d\omega \tag{35}$$

and

$$(\mathbf{T}_g)_{\text{mean}} = \frac{6\pi(\Delta I)}{T_n^2(1 - e^2)^{\frac{3}{2}}} \times\left[\mathbf{k}\cdot\int_0^{2\pi}\mathbf{i}_s\mathbf{i}_s(1 + e\cos\omega\cos P + e\sin\omega\sin P)\, d\omega \times \mathbf{k}\right]. \tag{36}$$

Since in the ORDEF coordinates (see Fig. 11)

$$\mathbf{i}_s = \cos \omega \mathbf{i}_g + \sin \omega \mathbf{j}_g \tag{37}$$

the dyad, $\mathbf{i}_s\mathbf{i}_s$ becomes

$$\mathbf{i}_s\mathbf{i}_s = \cos^2 \omega\, \mathbf{i}_g\mathbf{i}_g + \sin^2 \omega\, \mathbf{j}_g\mathbf{j}_g + \sin \omega \cos \omega(\mathbf{i}_g\mathbf{j}_g + \mathbf{j}_g\mathbf{i}_g). \tag{38}$$

Substituting this into (36) results in three integrals. Those containing $\mathbf{i}_g\mathbf{i}_g$ and $\mathbf{j}_g\mathbf{j}_g$ yield π as a result of the integration. The other integral is 0. Therefore,

$$(T_g)_{\text{mean}} = \frac{6\pi^2(\Delta I)}{T_n^2(1 - e^2)^{\frac{3}{2}}} [\mathbf{k} \cdot (\mathbf{i}_g\mathbf{i}_g + \mathbf{j}_g\mathbf{j}_g) \times \mathbf{k}]. \tag{39}$$

By some vector maneuvering (see Appendix A) this reduces to

$$(T_g)_{\text{mean}} = -\frac{6\pi^2(\Delta I)}{T_n^2(1 - e^2)^{\frac{3}{2}}} [(\mathbf{k} \cdot \mathbf{k}_g)(\mathbf{k}_g \times \mathbf{k})]. \tag{40}$$

To transform the ORDEF vectors into the SANOR system, we write

$$x_g = (CD)_i X \tag{22}$$

$$X = (\tilde{D}\tilde{C})x \tag{20}$$

$$\therefore\ x_g = (CD)(\tilde{D}\tilde{C})x. \tag{41}$$

Performing the indicated operations, after a bit of labor we find that

$$\begin{aligned}\mathbf{k}_g = {} & (\sin \Omega \sin i \cos \psi - \cos \Omega \sin i \sin \psi)\mathbf{i} \\ & + (-\sin \Omega \sin i \sin \psi \cos \theta - \cos \Omega \sin i \cos \psi \cos \theta + \cos i \sin \theta)\mathbf{j} \\ & + (\sin \Omega \sin i \sin \psi \sin \theta + \cos \Omega \sin i \cos \psi \sin \theta + \cos i \cos \theta)\mathbf{k}\end{aligned} \tag{42}$$

where, referring to Figs. 10 and 11, we see that

ψ = an Euler rotational angle

i = orbital inclination

Ω = ascending node of orbit.

Substituting into (40), the mean gravity torque reduces to

$$\begin{aligned}(\mathbf{T}_g)_{\text{mean}} = {} & \frac{6\pi^2\Delta I}{T_n^2(1 - e^2)^{\frac{3}{2}}} \{\cos i \cos \theta + \sin i \sin \theta \cos (\Omega - \psi)\} \\ & \cdot [\![(\sin i \cos \theta \cos (\Omega - \psi) - \cos i \sin \theta)\mathbf{i} + (\sin i \sin (\Omega - \psi))\mathbf{j}]\!].\end{aligned} \tag{43}$$

4.6 *The Mean Magnetic Torque*

It is well known[11] that the scalar potential (Φ_m) of a magnetic dipole

may be expressed as

$$\Phi_m = \frac{1}{4\pi\mu_0}\frac{\mathbf{p}\cdot\mathbf{i}_s}{r^2}$$

$$= \frac{1}{4\pi\mu_0}\frac{\mathbf{p}\cdot\mathbf{r}}{r^3} \tag{44}$$

$$= -\frac{p}{4\pi\mu_0}\frac{\mathbf{k}_m\cdot\mathbf{r}}{r^3} \tag{45}$$

where

μ_0 = permeability of free space
= $4\pi \times 10^{-7}$ webers/ampere-meter (Ref. 12)
= $4\pi \times 10^{-7}$ henry/meter (Ref. 12)
$\mathbf{p}$ = magnetic moment of earth's field, direction and magnitude
= 10^{17} weber-meters
= $10^{17}(10^{10}/4\pi)$ emu = 8.06×10^{25} emu
= 8.06×10^{25} erg/gauss (Ref. 12, p. 25)
$\mathbf{i}_s$ = unit vector along the x_s axis, local satellite vertical
r = distance from dipole center (earth's center) to satellite
$\mathbf{k}_m$ = unit vector describing direction of geomagnetic moment
p = magnitude of $\mathbf{p}$
$\mathbf{r}$ = vector form of r along i_s axis.

A satellite magnetic moment ($\mathbf{M}$) in the earth's magnetic field ($\mathbf{H}$) will produce a torque

$$\mathbf{T} = \mathbf{M} \times \mathbf{H}. \tag{46}$$

If the satellite spins rapidly, any magnetic moment components perpendicular to the spin axis will tend to produce torques which average to 0, while the component along the spin axis will produce a net torque of

$$\mathbf{T}_m = \mathbf{M}_s \times \mathbf{H} \tag{47}$$

$$= M_s\mathbf{k} \times \mathbf{H} \text{ ergs} \tag{48}$$

where

M_s = satellite magnetic moment along its spin axis (weber-meters or ergs/gauss)
$\mathbf{k}$ = unit vector along satellite spin axis (SANOR system)
$\mathbf{H}$ = geomagnetic field (ampere-turns/meters).

It is desired to integrate the instantaneous torque, $\mathbf{T}_m$, over one anomalistic period in order to calculate the mean torque. To do this,

we shall express **H** in the MAG system and eventually convert this expression into SANOR terms to be comparable with M_s.

We begin by setting

$$\mathbf{H} = -\nabla\Phi_m \tag{49}$$

from (45) and (49),

$$\mathbf{H} = -\frac{h}{\mu_0}\nabla\left[\frac{-\mathbf{k}_m\cdot(x_m\mathbf{i}_m + y_m\mathbf{j}_m + z_m\mathbf{k}_m)}{r^3}\right] \tag{50}$$

where

$$x_m, y_m, z_m = \text{components of } \mathbf{r} \text{ in MAG system}$$

and

$$h = p/4\pi. \tag{51}$$

Therefore,

$$\mathbf{H} = \frac{h}{\mu_0}\nabla(z_m/r^3) \tag{52}$$

and since

$$r^3 = (x_m^2 + y_m^2 + z_m^2)^{\frac{3}{2}}$$

we have

$$\mathbf{H} = \frac{-h}{\mu_0 r^5}[3x_m z_m\mathbf{i}_m + 3y_m z_m\mathbf{j}_m + (3z_m^2 - r^2)\mathbf{k}_m]. \tag{53}$$

Rewriting to spotlight **r** components, using the following relationships normalized to r,

$$x_m/r = r_x, \qquad y_m/r = r_y, \qquad z_m/r = r_z \tag{54}$$

one obtains

$$\mathbf{H} = -\frac{h}{\mu_0 r^3}[3r_x r_z\mathbf{i}_m + 3r_y r_z\mathbf{j}_m + (3r_z^2 - 1)\mathbf{k}_m] \tag{55}$$

or

$$\mathbf{H} = \frac{p}{4\pi\mu_0 r^3}[\mathbf{k}_m - 3(\mathbf{i}_s\cdot\mathbf{k}_m)\mathbf{i}_s] \tag{56}$$

since

$$\mathbf{r} = r\mathbf{i}_s. \tag{57}$$

By the following equations [(24) through (65)], the variables $\mathbf{i}_s$ and $\mathbf{k}_m$ will be expressed in forms useful in the ensuing mean magnetic torque calculations.

Let us first express $\mathbf{i}_s$ in the MAG system. As shown previously,

$$x_s = A_i X \tag{24}$$

and

$$X = (\tilde{D}\tilde{C})_\eta X_m \tag{27}$$

therefore

$$x_s = A_i(\tilde{D}\tilde{C})_\eta X_m \tag{58}$$

or

$$\begin{aligned}\mathbf{i}_s = {} & |\,(\cos\Omega\cos\omega - \cos i\sin\omega\sin\Omega) \\ & \cdot(\cos\omega\sin\Omega + \cos i\cos\Omega\sin\omega)(\sin\omega\sin i)\,| \\ & \times \begin{vmatrix} \cos\eta & -\sin\eta\cos\beta & \sin\eta\sin\beta \\ \sin\eta & \cos\eta\cos\beta & -\cos\eta\sin\beta \\ 0 & \sin\beta & \cos\beta \end{vmatrix} \begin{vmatrix} \mathbf{i}_m \\ \mathbf{j}_m \\ \mathbf{k}_m \end{vmatrix}.\end{aligned} \tag{59}$$

Expanding,

$$\begin{aligned}\mathbf{i}_s = {} & [\cos\eta(\cos\Omega\cos\omega - \cos i\sin\omega\sin\Omega) + \sin\eta(\cos\omega\sin\Omega \\ & + \cos i\cos\Omega\sin\omega)]\mathbf{i}_m + [-\sin\eta\cos\beta(\cos\Omega\cos\omega \\ & - \cos i\sin\omega\sin\Omega) + \cos\eta\cos\beta(\cos\omega\sin\Omega \\ & + \cos i\cos\Omega\sin\omega) + \sin\beta\sin\omega\sin i]\mathbf{j}_m + [\sin\eta\sin\beta \\ & (\cos\Omega\cos\omega - \cos i\sin\omega\sin\Omega) - \cos\eta\sin\beta(\cos\omega\sin\Omega \\ & + \cos i\cos\Omega\sin\omega) + \cos\beta\sin\omega\sin i]\mathbf{k}_m .\end{aligned} \tag{60}$$

This will be used later.

Also, $\mathbf{i}_s$ in the IS system may be written [see (24)] as

$$\mathbf{i}_s = A_i\mathbf{I} \tag{61}$$

$$\begin{aligned}\mathbf{i}_s = {} & [\cos\Omega\cos\omega - \cos i\sin\omega\sin\Omega]\mathbf{I} \\ & + [\cos\omega\sin\Omega + \cos i\cos\Omega\sin\omega]\mathbf{J} \\ & + [\sin\omega\sin i]\mathbf{K}.\end{aligned} \tag{62}$$

In a similar manner, $\mathbf{k}_m$ in the IS system is expanded as follows:

$$x_m = (CD)_\eta X \tag{63}$$

or

$$\mathbf{k}_m = \sin\eta \sin\beta\,\mathbf{I} - \cos\eta \sin\beta\,\mathbf{J} + \cos\beta\,\mathbf{K} \tag{64}$$

$$= \sin\beta(\sin\eta\,\mathbf{I} - \cos\eta\,\mathbf{J}) + \cos\beta\,\mathbf{K}. \tag{65}$$

The problem is now to integrate the instantaneous torque, $\mathbf{T}_m$, over one anomalistic period, T_a, to obtain the mean magnetic torque,

$$(\mathbf{T}_m)_{\text{mean}} = \frac{1}{T_a}\int_{t_i}^{t_i+T_a} \mathbf{T}_m dt = \frac{1}{T_a}\int_{v_i}^{v_i+2\pi} \mathbf{T}_m \frac{dt}{dv}\,dv = \frac{1}{T_a}\int_{v_i}^{v_i+2\pi} \mathbf{T}_m \frac{r^2}{h}\,dv \tag{66}$$

where

T_a = anomalistic period of the satellite
$\mathbf{T}_m$ = instantaneous magnetic torque
t = time
v = true anomaly of the satellite
r = geocentric satellite distance
h = defined by (68) below.

Substituting into (66) from (48) and (56)

$$(\mathbf{T}_m)_{\text{mean}} = \frac{M_s p}{4\pi\mu_0 T_a}\,\mathbf{k} \times \int_{v_i}^{v_i+2\pi} \frac{\mathbf{k}_m - 3(\mathbf{i}_s\cdot\mathbf{k}_m)\mathbf{i}_s}{r^3}\left(\frac{r^2}{h}\right) dv. \tag{67}$$

Since

$$h = \frac{2\pi a^2(1-e^2)^{\frac{1}{2}}}{T_a} \tag{68}$$[13]

and

$$r = \frac{a(1-e^2)}{1 + e\cos v} \tag{69}$$[13]

where

a = semimajor axis of orbit
e = orbital eccentricity
T_a = anomalistic period of the satellite

(67) becomes

$$(\mathbf{T}_m)_{\text{mean}} = \frac{M_s p}{8\pi^2 \mu_0 a^3 (1 - e^2)^{\frac{3}{2}}} \cdot \mathbf{k} \times \int_{v_i}^{v_i + 2\pi} [\mathbf{k}_m - 3(\mathbf{i}_s \cdot \mathbf{k}_m)\mathbf{i}_s](1 + e \cos v) dv \tag{70}$$

$$= \mathfrak{M}\mathbf{k} \times \int_{v_i}^{v_i + 2\pi} [\mathbf{k}_m - 3(\mathbf{i}_s \cdot \mathbf{k}_m)\mathbf{i}_s](1 + e \cos v) dv. \tag{71}$$

First we shall evaluate the integral of (71) beginning by substituting the $\mathbf{k}_m$ value given in (65), to obtain

$$\frac{(\mathbf{T}_m)_{\text{mean}}}{\mathfrak{M}} = (\sin \beta)k \times \int_{v_i}^{v_i + 2\pi} [\sin \eta \mathbf{I} - \cos \eta \mathbf{J} - 3\{\mathbf{i}_s \cdot (\sin \eta \mathbf{I} - \cos \eta \mathbf{J})\}\mathbf{i}_s](1 + e \cos v) dv \tag{72}$$

$$+ (\cos \beta)\mathbf{k} \times \int_{v_i}^{v_i + 2\pi} \{\mathbf{K} - 3(\mathbf{i}_s \cdot \mathbf{K})\mathbf{i}_s\}(1 + e \cos v) dv$$

$$= \text{I} + \text{II}. \tag{73}$$

Integral II, the simpler of the two, is evaluated in Appendix B. The result is given below:

$$\text{II} = \pi \cos \beta[\{-2 \sin \theta + 3 \sin^2 i \sin \theta + 3 \sin i \cos i \cos \theta \cos (\Omega - \psi)\}\mathbf{i} + 3 \sin i \cos i \sin (\Omega - \psi)\mathbf{j}]. \tag{88}$$

Now we must evaluate the first integral, I, of (73) but first let us state that by examining (72) it is perfectly obvious that the I integral does not exist for a noninclined dipole. For this case, it follows from (73) with $\cos \beta = 1$ that

$$(\mathbf{T}_m)_{\text{mean}} = \frac{M_s p}{8\pi^2 \mu_0 a^3 (1 - e^2)^{\frac{3}{2}}} \text{II}. \tag{89}$$

By suitable variable substitution the first integral I of (73) may be compressed to yield

$$\text{I} = (\sin \beta)\mathbf{k} \times (\mathbf{I}A - \mathbf{J}B - 3\mathbf{I} \cdot \mathbf{C} + 3\mathbf{J} \cdot \mathbf{E}) \tag{90}$$

where

$$A = \int_{v_i}^{v_i + 2\pi} \sin \eta (1 + e \cos v) dv \tag{91}$$

$$B = \int_{v_i}^{v_i+2\pi} \cos \eta(1 + e \cos v)dv \tag{92}$$

$$\mathbf{C} = \int_{v_i}^{v_i+2\pi} \mathbf{i}_s\mathbf{i}_s \sin \eta(1 + e \cos v)dv \tag{93}$$

$$\mathbf{E} = \int_{v_i}^{v_i+2\pi} \mathbf{i}_s\mathbf{i}_s \cos \eta(1 + e \cos v)dv. \tag{94}$$

Now η must be expressed as a function of v in order to evaluate A, B, $\mathbf{C}$, and $\mathbf{E}$. For simplification of the integrals we shall also let the initial time for the integration be the time when the satellite passes through perigee. Then

$$\eta = \eta_0 + \omega_E t \tag{95}$$

$$= \eta_0 + \omega_E T_a M/2\pi \tag{96}$$

$$= \eta_0 + bM \tag{97}$$

where

η_0 = initial position of the ascending node of the geomagnetic equator at perigee passage with respect to the IS system (see Fig. 12)
ω_E = angular velocity of the earth in the IS system
t = time measured from passage of satellite through perigee
M = mean anomaly of the satellite (radians)
T_a = anomalistic period of the satellite (time units)
$b = (\omega_E/2\pi)T_a$ = number of turns of earth in time T_a.

Therefore

$$\sin \eta = \sin \eta_0 \cos (bM) + \cos \eta_0 \sin (bM) \tag{98}$$

$$\cos \eta = \cos \eta_0 \cos (bM) - \sin \eta_0 \sin (bM). \tag{99}$$

Unfortunately, M is related to v through Kepler's equation as

$$M = E - e \sin E \tag{100}$$[14]

where

E = the eccentric anomaly
e = eccentricity of the orbit

and

$$E = 2 \tan^{-1}\left[\left(\frac{1-e}{1+e}\right)^{\frac{1}{2}} \tan \frac{v}{2}\right] = 2 \tan^{-1}\left(q \tan \frac{v}{2}\right). \tag{101}$$[14]

Equations (100) and (101) certainly define M as a function of v, but in a most complicated manner. It can be shown, however, that a plot of v and M versus time normalized to T_a will look like Fig. 14. So as a reasonable approximation to M we might consider

$$M = v - (\lambda/b) \sin v \tag{102}$$

where

λ/b = maximum amplitude of the true anomaly "sine" wave of Fig. 14 = $2e$.[15]

Note that (102) resembles Kepler's equation with v replacing E. With less sophistication we might even let

$$M = v. \tag{103}$$

The only justification here is that we shall be dealing in mean torques averaged over an orbital period, and the v function makes one oscilla-

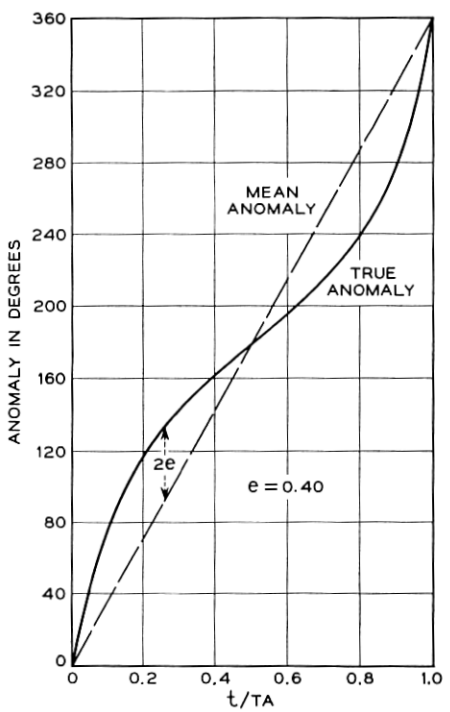

Fig. 14 — Mean and true anomaly comparison.

tion about the M function in that time. If (103) is assumed, (98) and (99) remain unaltered except that v replaces M. If (102) is used, (98) and (99) become

$$\begin{aligned}\sin \eta &= \sin \eta_0[\cos bv \cos (\lambda \sin v) + \sin bv \sin (\lambda \sin v)] + \\ &\quad \cos \eta_0[\sin bv \cos (\lambda \sin v) - \cos bv \sin (\lambda \sin v)] \qquad (104)\\ &= \sin \eta_0[A'] + \cos \eta_0[B'] \qquad (105).\end{aligned}$$

where A' and B' are defined by comparing (105) to (104). In like fashion,

$$\cos \eta = \cos \eta_0[A'] - \sin \eta_0[B']. \qquad (106)$$

We may express the sin $(\lambda \sin v)$ and cos $(\lambda \sin v)$ portions of A' and B' as

$$\sin (\lambda \sin v) \doteq \lambda \sin v - \frac{\lambda^3 \sin^3 v}{6} \qquad (107)$$

and

$$\cos (\lambda \sin v) \doteq 1 - \frac{\lambda^2 \sin^2 v}{2}. \qquad (108)$$

These approximations are reasonably valid for near earth satellites not having high eccentricities and avoid Bessel function complications. The neglect of higher-order terms in (107) and (108) for $e = 0.25$ and $T_a \doteq 150$ minutes results in errors of less than one part in 10^6.

As case I we shall evaluate the integrals A, B, $\mathbf{C}$, and $\mathbf{E}$ using (98) and (99) with v replacing M. For case II we shall return to evaluate these integrals again using (105), (106), (107), and (108). Case I details are given in Appendix C. Case II is outlined by Appendix D.

Using the expanded II integral of (88) and the evaluated A, B, $\mathbf{C}$, and $\mathbf{E}$ integrals from Appendices C and D, (73) may now be written as

$$\begin{aligned}(\mathbf{T}_m)_{\text{mean}} = \mathfrak{M}\Big[&\cos \beta\mathbf{k} \times \int_0^{2\pi} \{\mathbf{k} - 3(\mathbf{i}_s \cdot \mathbf{K})\mathbf{i}_s\}(1 + e \cos v)dv \\ &+ \sin \beta\mathbf{k} \times \{A\mathbf{I} - B\mathbf{J} - 3\mathbf{I}\cdot(\mathbf{i}_g\mathbf{i}_g C_1 + \mathbf{j}_g\mathbf{j}_g C_2 \\ &+ (\mathbf{i}_g\mathbf{j}_g + \mathbf{j}_g\mathbf{i}_g)C_3) + 3\mathbf{J}\cdot(\mathbf{i}_g\mathbf{i}_g E_1 + \mathbf{j}_g\mathbf{j}_g E_2 \\ &+ (\mathbf{i}_g\mathbf{j}_g + \mathbf{j}_g\mathbf{i}_g)E_3)\}\Big]\end{aligned} \qquad (130)$$

where

$A, B, C_1, C_2, C_3, E_1, E_2, E_3$ are all defined in Appendix C.

The following, expressed in the SANOR system, will now be substituted into (130) (refer to Fig. 11)

$$\mathbf{k} \times \mathbf{I} = \cos \psi \mathbf{j} + \sin \psi \cos \theta \mathbf{i} \tag{131}$$

$$\mathbf{k} \times (-\mathbf{J}) = \cos \psi \cos \theta \mathbf{i} - \sin \psi \mathbf{j} \tag{132}$$

$$\mathbf{J} \cdot \mathbf{i}_g = \sin \Omega \tag{133}$$

$$\mathbf{J} \cdot \mathbf{j}_g = \cos \Omega \cos i \tag{134}$$

$$\mathbf{I} \cdot \mathbf{i}_g = \cos \Omega \tag{135}$$

$$\mathbf{I} \cdot \mathbf{j}_g = -\sin \Omega \cos i \tag{136}$$

$$\mathbf{k} \times \mathbf{i}_g = -\cos \theta \sin (\Omega - \psi)\mathbf{i} + \cos (\Omega - \psi)\mathbf{j} \tag{137}$$

$$\mathbf{k} \times \mathbf{j}_g = (-\sin i \sin \theta - \cos i \cos \theta \cos (\Omega - \psi))\mathbf{i} - \cos i \sin (\Omega - \psi)\mathbf{j} \tag{138}$$

$$\mathbf{k} \times \mathbf{K} = -\sin \theta \mathbf{i}. \tag{139}$$

These yield the mean magnetic torque, which is

$$\begin{aligned}(\mathbf{T}_M)_{\text{mean}} = {} & \frac{M_s p}{8\pi^2 \mu_0 a^3 (1 - e^2)^{\frac{3}{2}}} \Big\{ \pi \cos \beta [\mathbf{i}\{-2 \sin \theta + 3 \sin^2 i \sin \theta \\ & + 3 \sin i \cos i \cos \theta \cos (\Omega - \psi)\} \\ & + \mathbf{j}\{3 \sin i \cos i \sin (\Omega - \psi)\}] \Big\} \\ & + \frac{M_s p \sin \beta}{8\pi^2 \mu_0 a^3 (1 - e^2)^{\frac{3}{2}}} \Big\{ A[\sin \psi \cos \theta \mathbf{i} + \cos \psi \mathbf{j}] \\ & + B[\cos \psi \cos \theta \mathbf{i} - \sin \psi \mathbf{j}] \\ & + 3[\{E_1 \sin \Omega + E_3 \cos \Omega \cos i - C_1 \cos \Omega \\ & + C_3 \sin \Omega \cos i\}\{-\cos \theta \sin (\Omega - \psi)\mathbf{i} \\ & + \cos (\Omega - \psi)\mathbf{j}\} + \{E_2 \cos \Omega \cos i + E_3 \sin \Omega \\ & + C_2 \sin \Omega \cos i - C_3 \cos \Omega\}\{-(\sin i \sin \theta \\ & + \cos i \cos \theta \cos (\Omega - \psi))\mathbf{i} - \cos i \sin (\Omega - \psi)\mathbf{j}\}] \Big\}\end{aligned} \tag{140}$$

or, collecting on $\mathfrak{M} \cos \beta$ and $\mathfrak{M} \sin \beta$,

$$\begin{aligned}(\mathbf{T}_M)_{\text{mean}} = {} & \pi \mathfrak{M} \cos \beta \Big[\mathbf{i}\{-2 \sin \theta + 3 \sin^2 i \sin \theta + 3 \sin i \cos i \\ & \cdot \cos \theta \cos (\Omega - \psi)\} + \mathbf{j}\{3 \sin i \cos i \sin (\Omega - \psi)\} \Big]\end{aligned} \tag{141}$$

$$+ \mathfrak{M} \sin \beta \Big[\mathbf{i} \Big\{ A \sin \psi \cos \theta + B \cos \psi \cos \theta - 3[\cos \theta \sin (\Omega - \psi)(E_1 \sin \Omega + E_3 \cos \Omega \cos i - C_1 \cos \Omega + C_3 \sin \Omega \cos i) + \{\sin i \sin \theta + \cos i \cos \theta \cos (\Omega - \psi)\}(E_2 \cos \Omega \cos i + E_3 \sin \Omega + C_2 \sin \Omega \cos i - C_3 \cos \Omega)] \Big\} + \mathbf{j} \Big\{ A \cos \psi - B \sin \psi + 3[\cos (\Omega - \psi)(E_1 \sin \Omega + E_3 \cos \Omega \cos i - C_1 \cos \Omega + C_3 \sin \Omega \cos i) - \cos i \sin (\Omega - \psi)(E_2 \cos \Omega \cos i + E_3 \sin \Omega + C_2 \sin \Omega \cos i - C_3 \cos \Omega)] \Big\} \Big].$$

Using the magnetic moment program, it has been shown in the case of the Telstar satellites that letting $M = v$ produces precessional results that follow the case II approximation over 1,000 orbits to within 0.01°. To document this result, the residual magnetic moment used was −0.9 microweber-meter, spin rate equaled 20 to 10 radians per second, spin axis and transverse moments of inertia were 4 slug-feet^2, orbit perigee was set to 4,500 miles, and eccentricity ranged from 0 to 0.95. Slight changes in the x-y torques of the order of thousandths of a microfoot pound were observed as the principal differences in the case I and II approximations for these eccentricity ranges. While these differences are negligible for the Telstar I and II satellites, other satellites in sufficiently lower orbits or having greater residual magnetic moments could require the case II approximation (no complete study has been made to date to bound the required ranges of the above mentioned variables for case I to achieve agreement to within 0.01° of case II).

4.7 *Equations of Motion of a Body Symmetrical about Its Spin Axis*[16]

The mean gravity and magnetic torque equations have been derived in the previous section. To analyze the motion of a spin-stabilized satellite responding to these torques, certain gyroscopic equations must now be developed. We begin by relating the vector angular momentum, $\mathfrak{H}$, for any rotating body to the external forces acting on the body as

$$\mathfrak{H}' = \mathbf{N} \tag{142}$$

where

$\mathbf{N}$ = resultant moment of all external forces acting on the body
$\mathfrak{H}'$ = the time derivative of $\mathfrak{H}$.

Using the assumptions in 4.3, we write in the SANOR system

$$\mathcal{H} = \dot{\varphi} I_3 \mathbf{k} \tag{143}$$

where

$\dot{\varphi}$ = the satellite spin rate.

From this, it follows that (see Fig. 10)

$$\mathcal{H}' = I_3[\ddot{\varphi}\mathbf{k} + \dot{\varphi}(\boldsymbol{\omega} \times \mathbf{k})] \tag{144}$$

where

$\boldsymbol{\omega}$ = angular velocity of the SANOR system referenced to IS coordinates.

We may express $\boldsymbol{\omega}$ in the SANOR system as (see Fig. 10)

$$\boldsymbol{\omega} = \omega_x \mathbf{i} + \omega_y \mathbf{j} + \omega_z \mathbf{k} \tag{145}$$

or

$$\boldsymbol{\omega} = \dot{\theta}\mathbf{i} + \dot{\psi} \sin \theta \mathbf{j} + \dot{\psi} \cos \theta \mathbf{k} \tag{146}$$

where

ω_x, ω_y, ω_z = angular velocity about the a, y, and z axes respectively.

Combining (142), (144), and (146), after performing the indicated operations

$$\mathbf{N} = I_3(\dot{\varphi}\dot{\psi} \sin \dot{\theta}\mathbf{i} - \varphi\dot{\theta}\mathbf{j} + \ddot{\varphi}\mathbf{k}). \tag{146}$$

Expressing (146) as x, y, and z torques in the SANOR system,

$$T_x = I_3\dot{\varphi}\dot{\psi} \sin \theta \tag{147}$$

$$T_y = -I_3\dot{\varphi}\dot{\theta} \tag{148}$$

$$T_z = I_3\ddot{\varphi}. \tag{149}$$

Quite obviously it is the x and y torques which produce precession. These torques, by the assumptions of Section IV, are the sums of the x and y components of the gravity and magnetic torques expressed by (43) and (141). T_z is zero as a result of assuming zero magnetic moment transverse to the spin axis and mass symmetry about that axis. We note that a nonzero T_z implies a change in the spin rate. For the Telstar I and II satellites this takes place principally because of induced eddy currents which produce transverse moments.*

* The general equations of motion referred to the center of mass for a rigid body spinning about the z axis, and symmetrical about this axis, are

4.8 *Alternate Inertial Coordinate System*

Clearly, (143) is valid only if the angular momentum vector, $\mathfrak{K}$, coincides with the satellite spin axis **k**. We note in (147), which was derived from (143), that the above assumption will be approximated only if $\dot{\psi} \sin \theta$ is small as compared to $\dot{\varphi}$. Otherwise the direction of $\mathfrak{K}$ shall certainly be influenced by that term as well as $\dot{\varphi}$. We note too that a valid condition within the bounds of the assumption is for $\dot{\psi} \sin \theta$ to be small even with large $\dot{\psi}$ provided only that θ itself be appropriately small. That is, solutions to the equation of motion exist for large $\dot{\psi}$, and those will occur only for small θ because of (143).* But if θ be near 0° or 180°, a singularity exists in (147), for $\dot{\psi}$, as a result, approaches infinity. An exit from this dilemma may be secured simply by transforming to a new reference set of inertial coordinates in place of the IS system whenever θ becomes small. Naturally, the new set should be chosen so that the equivalent θ then existing will be large. This is accomplished by redefining IS so that

$$X_2 \text{ corresponds to } Y$$

$$Y_2 \text{ corresponds to } Z$$

$$Z_2 \text{ corresponds to } X$$

as shown in Fig. 15. Let us call this new inertial frame the IS2 system.

Transformation equations to relate IS to IS2 are quite simple and are given below:

$$X_2 = QX \tag{150}$$

$$X = \tilde{Q}X_2 \tag{151}$$

$$T_x = I\ddot{\theta} + (I_3 - I)\dot{\psi}^2 \sin \theta \cos \theta + I_3\dot{\varphi}\dot{\psi} \sin \theta$$

$$T_y = I\ddot{\psi} \sin \theta + (2I - I_3)\dot{\psi}\dot{\theta} \cos \theta - I_3\dot{\varphi}\dot{\theta}$$

$$T_z = I_3(\ddot{\psi} \cos \theta - \dot{\varphi}\dot{\theta} \sin \theta + \ddot{\varphi}).$$

For cases where $\dot{\varphi}$ dominates , $\dot{\theta}\dot{\psi}$ sin θ, and $\dot{\psi}$ cos θ, these torques reduce to those given by (147), (148) and (149). We note principally that a change in spin rate reflects a T_z processional torque, from the above equations, but this is generally small and is neglected in this paper. For Telstar I, this torque component is estimated at least two orders of magnitude below the magnetic torques considered herein. (See also Ref. 17.)

* This is the case for precession through or near the north or south celestial pole, where even small changes in attitude, or θ, can produce large changes in ψ. The situation is quite analogous to an azimuth-elevation antenna tracking a satellite that passes through or near the zenith, where the azimuth rates become extremely high even for small changes in satellite position.

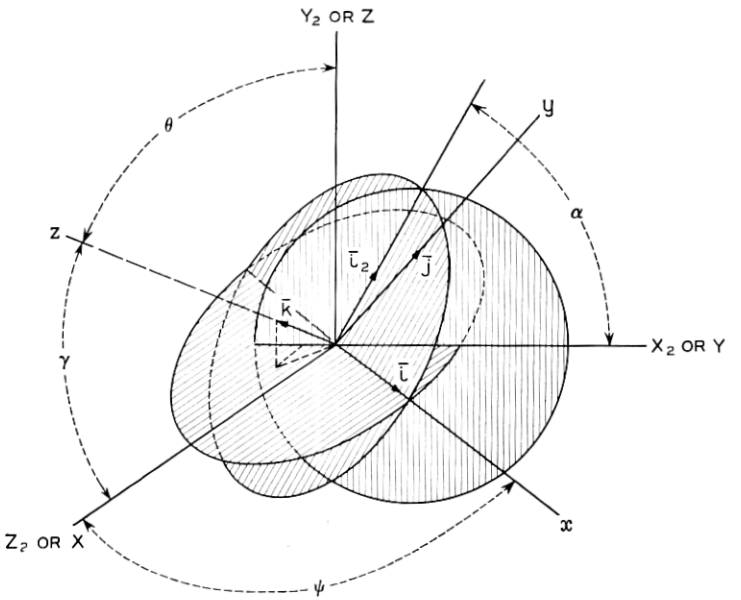

Fig. 15 — Euler rotations in the alpha-gamma system.

where

$$Q = \begin{vmatrix} 0 & 1 & 0 \\ 0 & 0 & 1 \\ 1 & 0 & 0 \end{vmatrix} \tag{152}$$

and

$$\tilde{Q} = \begin{vmatrix} 0 & 0 & 1 \\ 1 & 0 & 0 \\ 0 & 1 & 0 \end{vmatrix}. \tag{153}$$

Relationships between the other coordinate systems and the IS2 system may be obtained using equations of Section 4.4 and applying the Q matrix as appropriate, except that in the expanded matrices

$$\alpha \text{ corresponds to } \psi$$

$$\gamma \text{ corresponds to } \theta$$

where

α = The Euler angle measured from X_2 to the intersection of the xy and X_2Y_2 plane, which defines a new x axis called the x_2 axis in a SANOR 2 system. (See Fig. 15.)

γ = The Euler angle measured from Z_2 to **k** in a plane perpendicular to the x_2 axis. (Rotation is about the x_2 axis.)

Quite obviously, the steps leading to the mean gravity and mean magnetic torques may be retraced using the Q matrix and the new α,γ Euler angles. This would lead to torque expressions as functions of these desired angles. The same result may be obtained by transforming the final torques expressed in the ψ-θ system to expressions in the α-γ system by using explicit relationships between these two systems. We shall choose this later route and the needed relationships will now be derived.

We note in Fig. 15 that the **k** (satellite spin) vector remains in the same spatial position whether expressed in the IS or IS2 system. It seems reasonable then to proceed to relate α-γ to ψ-θ by observing the projections of the **k** vector on the XY and X_2Y_2 planes, respectively.

Referring to Fig. 16, we see that

$$\tan \alpha = \frac{-\sin \theta \cos \psi}{-\cos \theta} \tag{157}$$

$$\cos \gamma = \sin \theta \sin \psi \tag{158}$$

$$\sin \gamma = (1 - \sin^2 \theta \sin^2 \psi)^{\frac{1}{2}}. \tag{159}$$

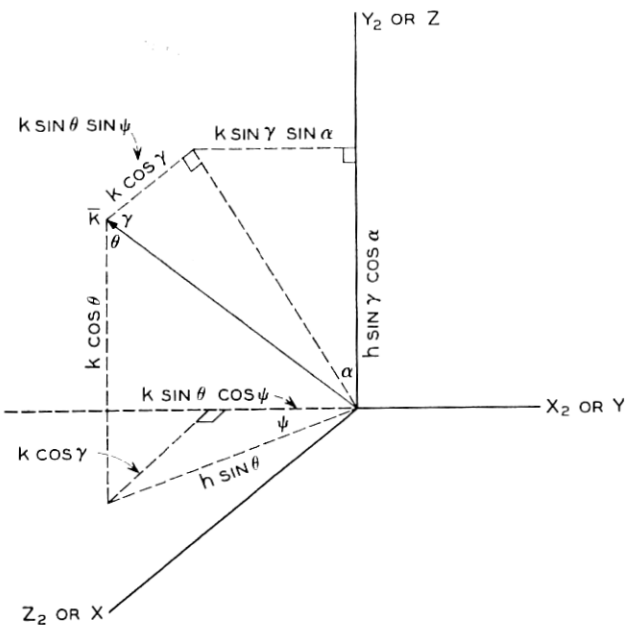

Fig. 16 — Theta-psi and alpha-gamma geometric relationships.

Quite obviously, inverse relationships may be developed. These are

$$\tan \psi = \frac{\cos \gamma}{-\sin \alpha \sin \gamma} \tag{160}$$

$$\cos \theta = -\cos \alpha \sin \gamma \tag{161}$$

$$\sin \theta = (1 - \cos^2 \alpha \sin^2 \gamma)^{\frac{1}{2}}. \tag{162}$$

4.9 *Mean Gravity and Magnetic Torques — Alternate Euler Rotations*

Using (157) through (159) it can be shown that the mean gravity torque expressed in the α-γ system is

$$\begin{aligned}(\mathbf{T}_G)_{\text{mean}} = \frac{6\pi^2 \Delta I}{T_n^2 (1 - e^2)^{\frac{3}{2}}} \Big\{ & (-\sin \Omega \sin i \cos \gamma \\ & + \cos \Omega \sin i \sin \alpha \sin \gamma + \cos i \cos \alpha \sin \gamma) \Big\} \\ & [\mathbf{i}_2(\sin \Omega \sin i \sin \gamma + \cos \Omega \sin i \sin \alpha \cos \gamma \\ & + \cos i \cos \alpha \cos \gamma) + \mathbf{j}_2(\cos \Omega \sin i \cos \alpha \\ & - \cos i \sin \alpha)]. \end{aligned} \tag{163}$$

Likewise, the mean magnetic torque can be expressed as

$$\begin{aligned}(\mathbf{T}_m)_{\text{mean}} = {} & \pi \mathfrak{M} \cos \beta \Big[\mathbf{i}_2 \Big\{ -2 \cos \alpha \cos \gamma + 3 \sin i (\sin i \cos \alpha \cos \gamma \\ & - \sin \Omega \cos i \sin \gamma - \cos \Omega \cos i \sin \alpha \cos \gamma) \Big\} \\ & + \mathbf{j}_2 \Big\{ 2 \sin \alpha - 3 \sin i (\sin i \sin \alpha \\ & + \cos \Omega \cos i \cos \alpha) \Big\} \Big] \\ & + \mathfrak{M} \sin \beta \Big[\mathbf{i}_2 \Big\{ -A \sin \gamma \\ & - B \sin \alpha \cos \gamma + 3G_1 (\sin \Omega \sin \alpha \cos \gamma \\ & - \cos \Omega \sin \gamma) + 3G_2 (-\sin i \cos \alpha \cos \gamma \\ & + \sin \Omega \cos i \sin \gamma + \cos \Omega \cos i \sin \alpha \sin \gamma) \Big\} \\ & + \mathbf{j}_2 \Big\{ -B \cos \alpha + 3G_1 \sin \Omega \cos \alpha \\ & + 3G_2 (\sin i \sin \alpha + \cos i \cos \Omega \cos \alpha) \Big\} \Big] \end{aligned} \tag{164}$$

where

$$G_1 = E_1 \sin \Omega + E_3 \cos \Omega \cos i - C_1 \cos \Omega + C_3 \sin \Omega \cos i \tag{165}$$

$$G_2 = E_2 \cos \Omega \cos i + E_3 \sin \Omega + C_2 \sin \Omega \cos i - C_3 \cos \Omega. \tag{166}$$

All other terms have meanings described previously.

V. EXPERIMENTAL RESULTS — GENERAL

Using the methods described herein, the attitudes of the Telstar I and II satellites have been predicted, determined, and these two results compared. In the case of the Telstar I satellite, the maximum angular deviation between predicted and determined attitude is 0.90° with the special-case exception of pass 2154, which is covered in detail later.* The average angular deviation is 0.38°. The predicted attitude of the Telstar II satellite deviates from that determined by optical flashes and solar sensors by a maximum of 0.5° and an average of 0.09°. These results are tabulated in Tables II and III. Here the deviation in right ascension and declination is displayed by subtracting the predicted values from the determined values. The angular deviation between predicted and determined attitude is also given as the celestial great circle arc G. When this value is followed by N, this indicates that no attitude fix has been determined by loci intersections (see Section II), and so the shortest arc distance between the corresponding attitude locus and the prediction is quoted. The T preceding an attitude determination indicates the selection of that point as a target toward which a magnetic moment program embodying the above analysis attempts to converge.

5.1 *Experimental Results — The Telstar I Satellite*

The Telstar I satellite entered orbit on July 10, 1962. Its attitude, calculated by combining nominal third-stage burnout parameters and stage 1 and 2 telemetry data, is given in Table I. Between launch and pass 16, there were a number of instances when the orientation coil was inadvertently energized by misinterpreted command signals sent to the satellite at extreme ranges and/or low elevations. This orientation coil (often referred to as a "torque coil") is located in the equatorial plane of the Telstar satellite just under the outer skin. Its purpose is to enable attitude adjustments by the production of a magnetic moment whenever current is sent through the coil. A fixed amount of current may be caused to flow in either direction through the coil so as to produce a magnetic moment, in addition to the residual moment, of ± 7.8540 microweber-meters. Fig. 17 diagrams the sense of the magnetic vectors which are called positive, indicates the resulting north and south magnetic poles of the satellite, and shows the corresponding positive direction of the current flow in the orientation coil. The relative magnetic directions and current flow are in accord with established standards.

* There are apparent exceptions on passes 16, 72 and 1657, but these relate to antenna pattern techniques (see Section 5.1) which have an expected accuracy of $\pm 1°$ to $\pm 2°$.

TABLE II—TELSTAR I SATELLITE—ATTITUDE COMPARISON

Pass Number	Attitude Determination		Type Data for Determ.	Attitude Prediction		Deviation (Det.—Predict.)			MAG MOM (MWM)
	RA	DEC		RA	DEC	RA	DEC	G	
Burnout				83.7	−66.8				
16	84.2	−65.8	SM	84.2	−65.18	0	0	0	−0.86328
16	83.0	−66.0	A	84.2	−65.18	−1.2	−0.82	1.4	
72				87.78	−66.27			0.5N	
72	86.0	−67	A			−1.3	−0.73	1.2	
135-136	91.7	−66.0	M	92.19	−66.36	−.49	0.36	0.6	
199	single locus		M	96.49	−65.95			0.4N	
271	100	−65	A	100.80	−64.92	−0.8	−0.8	0.5	
272	single locus		M	100.90	−64.90			0.6N	
272	↓	↓	S	100.90	−64.90			0.2N	
472				107.50	−59.80			0.2N	
931	T100.5	−49.84	M	100.74	−49.93	−0.24	0.09	0.18	↓
									−0.86328
1051	single locus			97.25	−50.21			0.9N	+6.9907
									−0.86328
1069				98.42	−49.70			0.6N	−8.7173
1114				95.92	−51.01			0.1N	−0.71103
1430				92.62	−59.55			0.1N	↓
1567	T96.2	−64.2	M	96.71	−64.21	−0.51	−0.01	0.23	↓
									−0.71103
1657	99.2	−67.0	A	102.81	−66.64	−3.61	0.36	1.7	7.14297
									−0.59101
1695				78.58	−57.01				
1909				90.59	−59.71			0.7N	
2154-55	T104.0	−53.5	M	104.71	−54.81	−0.71	−1.3	1.5	
2200	single locus			106.03	−53.28			0.1N	
2264				107.20	−50.74			0.4N	
2464				107.09	−43.65			0 N	
2482				106.88	−43.04			0 N	
2509				106.57	−42.33			0 N	
2582-83	105.2	−40.2	M	105.44	−40.53	−0.24	0.38	0.4	
3340, 41, 42	106.3	−43.7	M	103.68	−61.54	−2.62	17.8	18.0	
3476-7	112.30	−46.32	M	120.21	−66.21	7.91	19.9	22.0	
3495				123.16	−66.41				
3476-7	T112.30	−46.32	M	112.30	−46.32†	0	0	0	−0.40945

M = Mirror flash data.
A = Antenna pattern data.
S = Solar sensor data.
† Connects 3340 to 3476.

Data relating to the inadvertent uses of the orientation coil are insufficient to reconstruct the detailed precessional motion of Telstar I from launch to pass 16. Cn pass 16, however, an attitude determination was made by reducing optical and solar sensor data. This along with an attitude fix on pass 135–136 made from mirror flash data indicated a magnetic moment of about −0.7 microweber-meter. This was later refined to −0.86328 microweber-meter by causing the magnetic moment program to connect, by the precessional theory herein described, the

TABLE III—TELSTAR II SATELLITE—ATTITUDE COMPARISON

Pass Number	Attitude Determination		Type Data	Attitude Prediction		Deviation (Det.-Predict.)			MAG MOM (MWM)
	RA	DEC		RA	DEC	ΔRA	ΔDEL	G	
Burnout				82.23	−57.31				
62, 63, 63	87.75	−55.08	M	87.75	−55.08	0	0	0	−0.48375
100				88.55	−55.05	0	0	0	−0.48375
132, 133, 133	88.75	−55.34	M	89.23	−54.97	−0.48	−0.37	−0.5	
281				92.17	−54.10			0N	
293, 293	92.3	−54.05	M	92.38	−53.99	−0.08	−0.06	0.1	
324, 25	92.40	−53.71	M	92.90	−53.71	0	0	0	
331				93.01	−53.66			0.08N	
490				94.95	−51.81				
496	T95.00	−51.73	M	95.00	−51.73			0N	
541				95.34	−51.10			0N	
573				95.49	−50.74			0N	
611				95.63	−50.20			0.13N	
643				95.71	−49.80			0.16N	

M = Mirror flash data.
S = Solar sensor data.

attitude on pass 16 to a point on the pass 931 attitude locus. The convergence is within 0.18°, as shown in Table II. Using this latter magnetic moment, the precessional motion from passes 16 to 1051 was established. This precessional history is given in Fig. 18, where both the predicted curve and the attitude loci data are displayed.

When an optical flash series is recorded at the Holmdel Laboratories, the midpoint of that series can be determined with a time accuracy of less than ±20 seconds when using visual observation through the on-site telescopes and within ±10 seconds photoelectrically. The early data recorded on the Telstar I satellite did not indicate the expected accuracy at the midpoints, so in Fig. 18 only central loci are plotted. We must therefore think of these loci as having possible tolerances up to ±10 seconds, since photoelectric data were reduced. A tolerance of ±10 seconds can cause the maximum locus limit to be displaced as much as ±0.7° on either side of the plotted central loci. Considering this, the predicted attitude curve passes through every loci and every loci intersection on Fig. 18 with the single exception of pass 1051. The prediction curve would miss the lower limit of this locus by 0.3°.

Extended attitude predictions were made on October 1, 1962 (around pass 800) and covered the period through January 22 (pass 1800). These indicated that attitude adjustments should be initiated during

January, 1963. This was needed to prevent the solar offset from exceeding about 15° as required (see Section I). In order to check the attitude correction procedures, a test maneuver was initiated on pass 1051. It began by turning on the orientation coil, so as to produce a magnetic moment of +7.8540 microweber-meters to oppose the −0.86328 residual moment and yield a resultant of +6.9907 microweber-meters. This was continued through pass 1058, whereupon the coil was turned off until pass 1069. On 1069 the coil was turned on in the opposite sense so as to produce a moment of −7.8540 microweber-meters, giving the satellite a net moment of −8.7173 microweber-meters. On pass 1075, the coil was turned off. All told, the coil was positive for about 18 hours and negative for about 16 hours, a fact which approximately nullified the

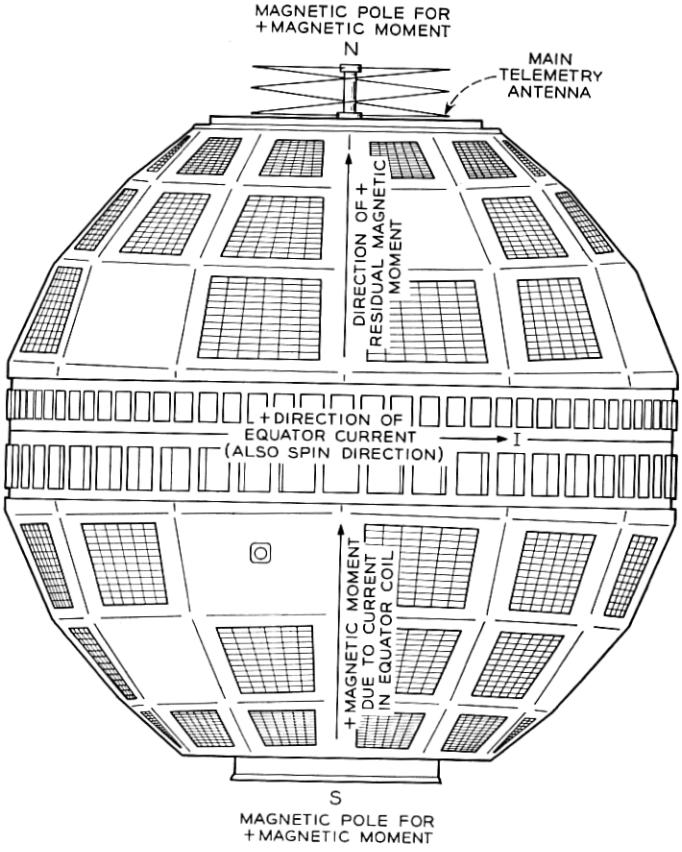

Fig. 17 — Direction of positive magnetic moments for Telstar satellites.

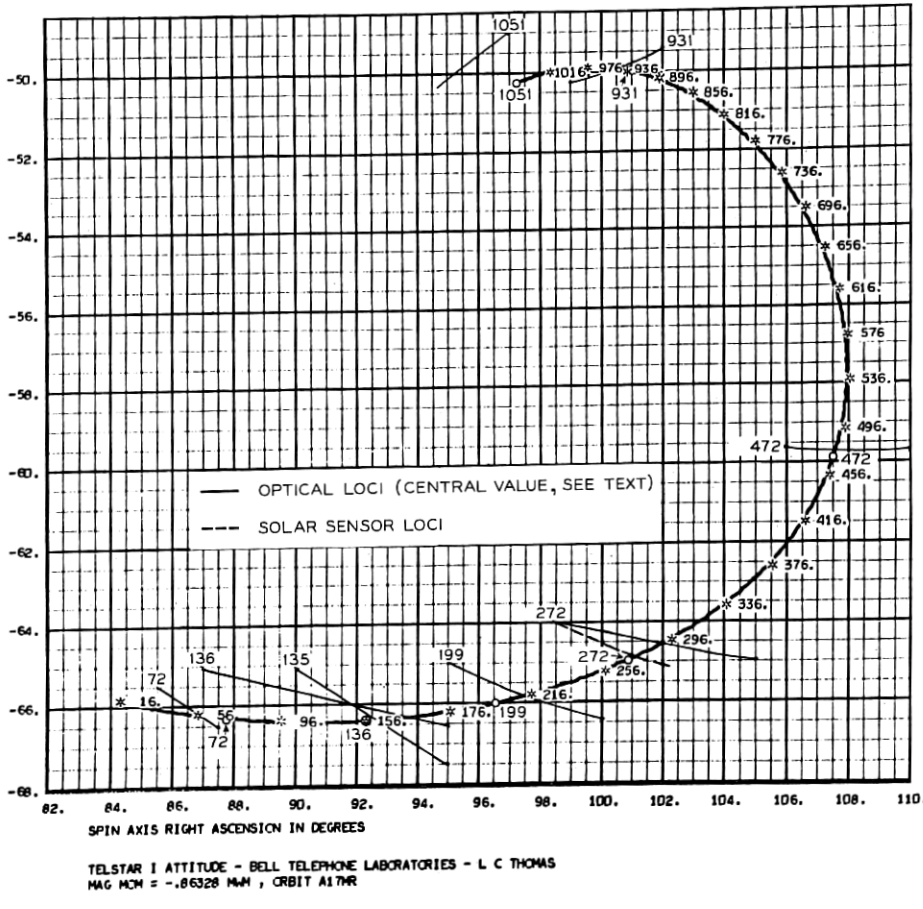

Fig. 18 — Telstar I precessional history — passes 16 through 1051.

precessional effect of the coil as intended for this test. Details of this maneuver are shown in Fig. 19.

Table II summarizes the agreement of loci to prediction during this period. Giving loci of unknown tolerances a $\pm 0.7°$ spread and using the known tolerance for pass 1114, the residuals shown in Table IV are produced.

The magnetic moment program connected the attitude on pass 1075 to that determined by mirror data on pass 1567 within 0.23°. In so doing, it calculated a residual magnetic moment of -0.71103 micro-weber-meter for that era. Using this calculated moment, predictions are extended to pass 1657 where, on January 7, 1963, the main orientation

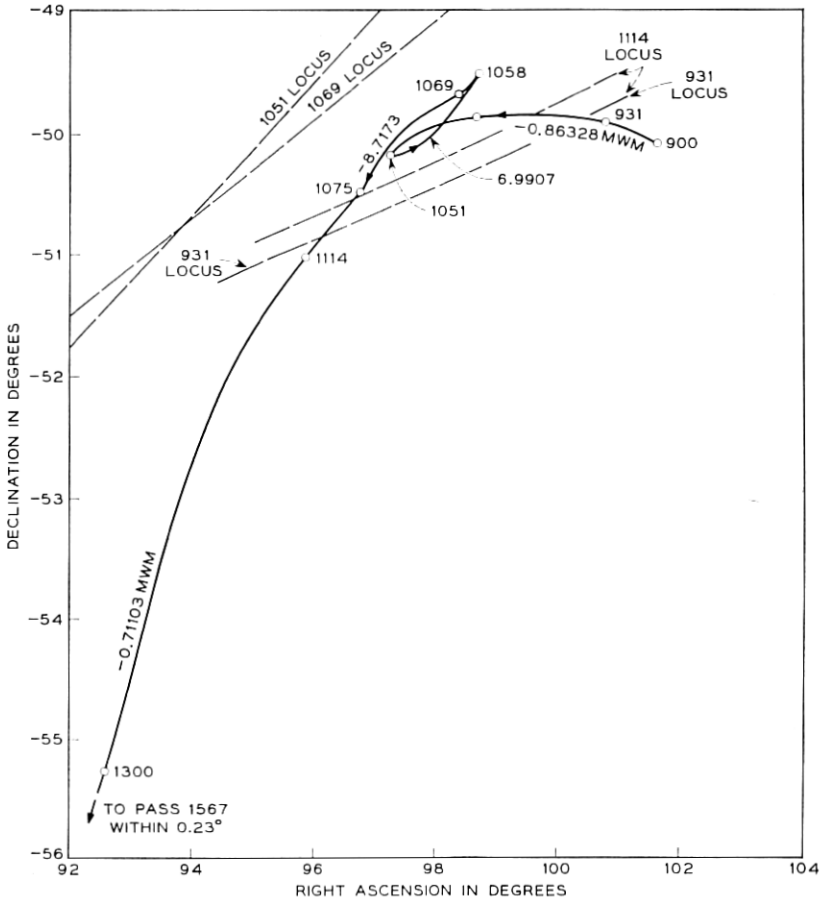

Fig. 19 — Details of the trial torqueing maneuver.

TABLE IV — TELSTAR I SATELLITE — TEST MANEUVER

Pass Number	Deviation of Prediction from Optical Locus
1051	0.3°
1069	0°
1114	0.1°

maneuver began. The region from pass 1075 to 1657 is shown in Fig. 20 along with the attitude loci. Predictions fit the determinations throughout within about 0.2°.

In addition to using mirror flash and solar sensor data to determine attitude, W. C. Jakes, Jr. and group at the Holmdel Laboratories deduced the attitude for a number of passes in this period by analyzing antenna pattern data.[18] Some of these determinations are included in Table II. Since their expected accuracy is ±1°, these data also serve to corroborate the predicted attitude.

The orientation coil was energized for the major attitude maneuver

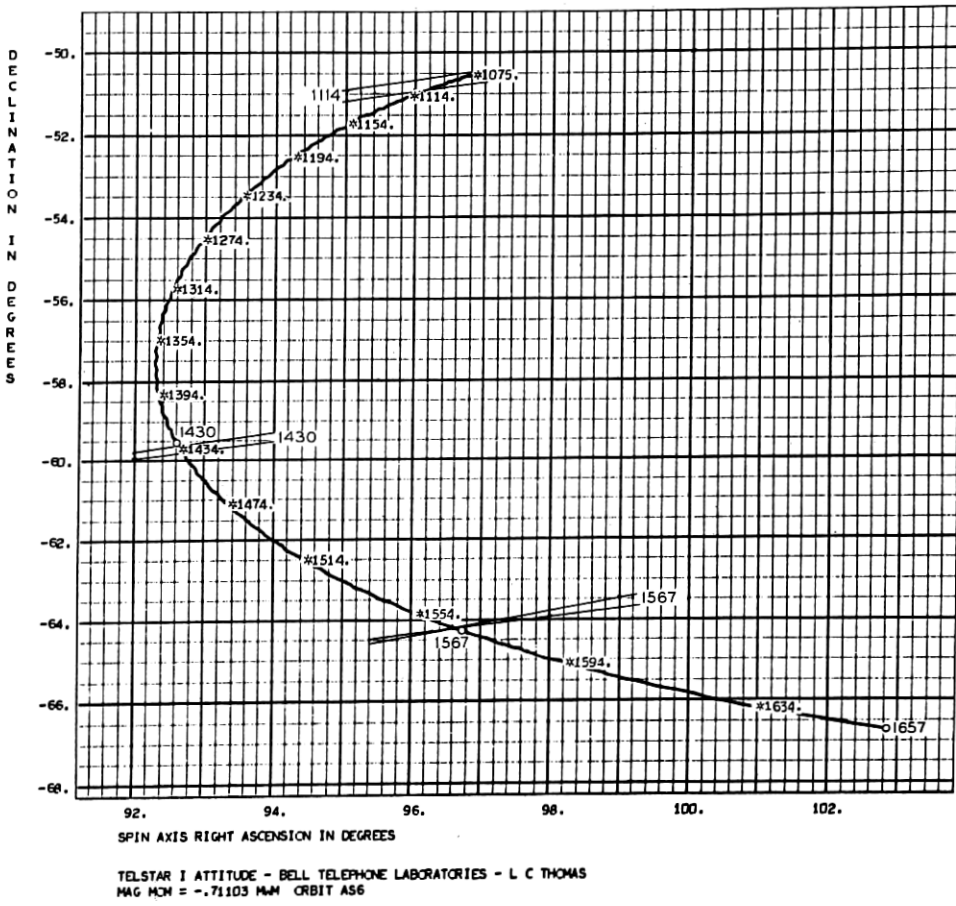

Fig. 20 — Telstar I precessional history — passes 1075 to 1657.

beginning on pass 1657, January 7, 1963, and ending on pass 1695, January 11, 1963. During this time the residual magnetic moment of −0.71103 microweber-meter had superimposed upon it a 7.8540 microweber-meter moment as a result of the coil. The attitude of the Telstar I satellite was changed by over 20° during this maneuver. The attitude and curve for this period are given in Fig. 21. The slight ripples in these curves are due to the inclination of the earth's dipole. Because of the small scale of this plot, these ripples are more noticeable than in the previous graphs.

At this point, we might well insert a brief discussion of the planning

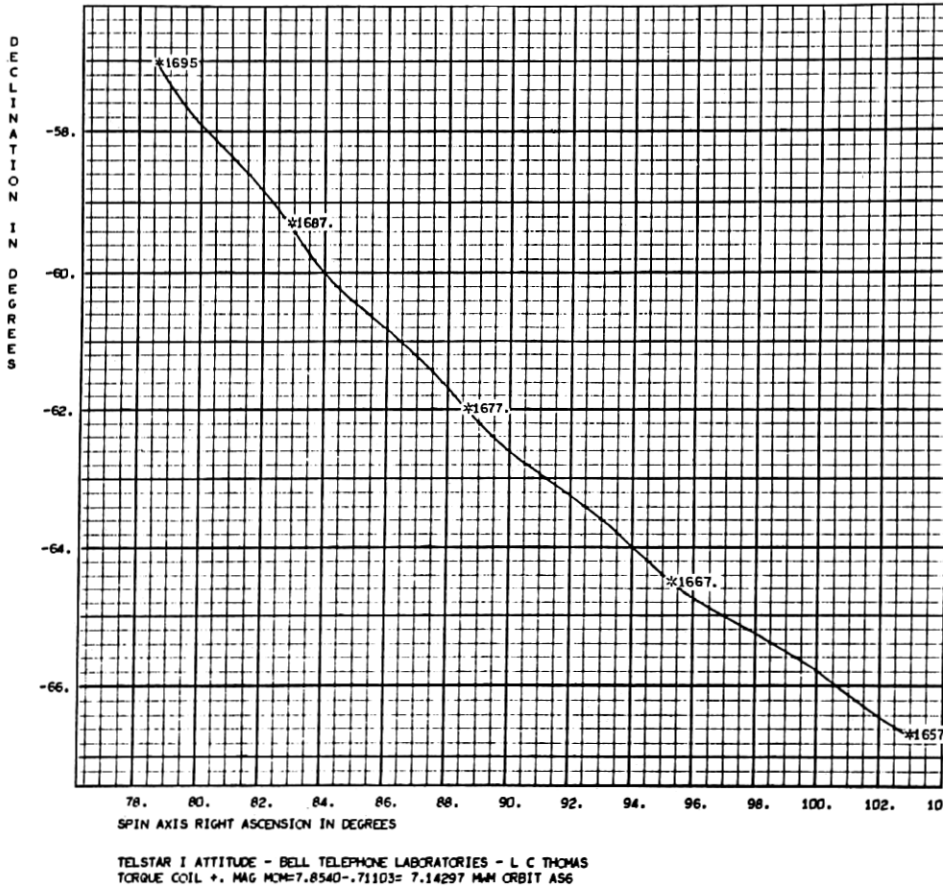

Fig. 21 — Telstar I precessional history — passes 1657 to 1695.

behind this attitude maneuver and why pass 1657 was chosen for its commencement. First of all, it can be shown that for any angular offset in the spin axis from a fixed, desired orientation there exists, for each instant in time, a determinable polarity of voltage for the equatorial coil which will tend to decrease the offset. To utilize this principle fully would require turning on the orientation coil on many occasions when the Telstar I satellite entered the Andover skies. While such a procedure would tend to decrease the angular offset generally in the most direct fashion, there are occasions in the lifetime of the Telstar satellite when leaving the coil on for a number of revolutions will produce faster corrections than pulsing the coil continually at Andover. This is because the instantaneous torque produced by the continuous magnetic moment of the coil in the earth's magnetic field varies during an orbital period in such a way that, in general, the average value exceeds the torque obtainable by energizing the coil only in the Andover skies. The optimum procedure then is for a period of continuous operation and this was undertaken. Fig. 22 shows the results of turning on the coil for steady torqueing at various dates. The heavy spiral shows the predicted position of the spin axis in right ascension and declination if the coil is never energized (the trial maneuver is omitted here for simplicity). The diverging curves indicate the motion due to the torqueing coil. Examination of Fig. 22 shows rapid precession as a result of the torque coil field, so that no mode of continuous coil operation will long permit the spin axis to point close to the south ecliptic pole. The solar offset also must ultimately increase with the enlarging ecliptic angle. It therefore follows that if a simplified mode of coil operation exists, it must begin with a relatively short period of coil operation.

Two factors concerning the precessional motions are noted in Fig. 22. They are:

(*i*) All precessional motions involving the orientation coil lie outside the spiral of residual precession for many orbits, because the net magnetic moment existing when the coil is actuated exceeds the residual magnetic moment.

(*ii*) Torque coil precession for both positive and negative coil polarity begins incrementally at the spiral in opposite directions.

We see that the torque coil should be used sparingly, because of the relatively rapid motion it produces. The problem that remains is to determine the times to turn on and turn off this coil and also to investigate whether or not future coil use is required. Because the spin rate of the satellite is decreasing, equal magnitudes of satellite magnetic moments will cause greater and greater precessional motion as time passes.

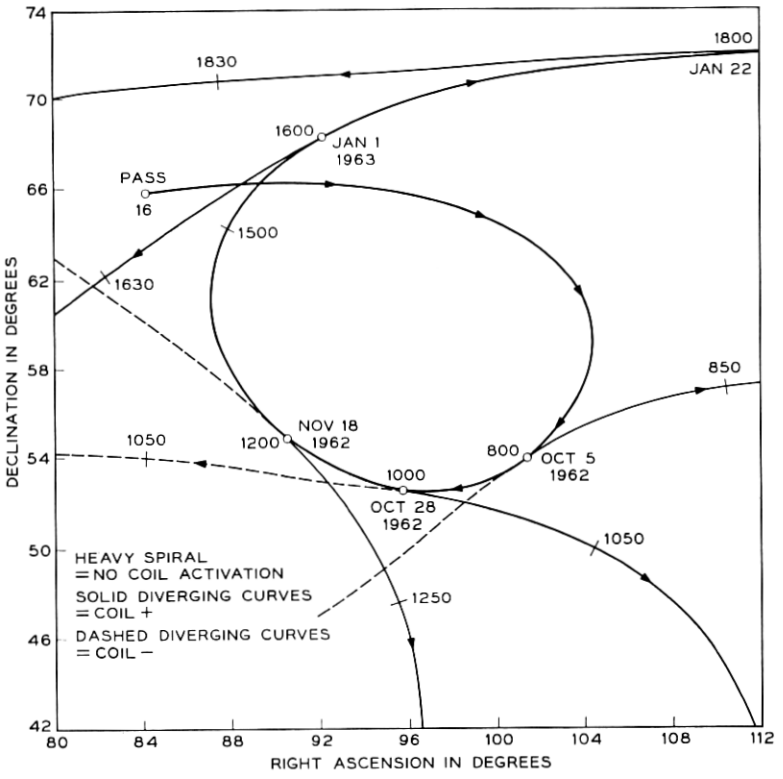

Fig. 22 — Telstar I predicted attitude showing steady torqueing.

It is to be expected that after the coil is actuated and then turned off a spiral of larger excursion than that occurring for passes 16 through 1655 will result strictly because of the lower spin rate existing at the later time. There is no way to avoid this except by repeated coil pulsing.

To avoid, or at least minimize, repeated coil usage, the procedure is to try to keep the maximum ecliptic angle as small as possible. If this value is expected to exceed the allowable solar offset, it is advantageous to time the operation so that the maximum ecliptic angle will occur at the time of minimum solar offset. This criterion governs both the selection of the day for coil turn-on as well as the duration of the attitude maneuver. As may be guessed from Fig. 22 and from the precessional motion factors stated above, only short torqueing operations during the month of January would result in the next precessional spiral (after coil turn-off) returning anywhere near the initial spiral shown in Fig. 22.

To cause the maximum ecliptic angle and the minimum solar offset to occur together, orientation coil use had to begin in the period from January 1 to January 7, 1963. As shown above, the maneuver which did begin on January 7 placed the attitude at right ascension 78.6° and declination at 57.0° by pass 1695.

The magnetic moment program, in connecting pass 1695 attitude to that determined by mirror data on passes 2154 and 2155, determined a residual magnetic moment of −0.59101 microweber-meter. This differs by about 0.1 microweber-meter from the residual moment going into the torqueing maneuver, but appears to be borne out by the closeness of fit to the mirror data from pass 1695 through pass 2583 (see Table II).* Fig. 23 plots this trajectory along with the mirror loci. The fit of attitude predictions to determinations is very good from passes 1695 through 2583 (see Table II). The largest deviation of 1.5° on passes 2154–2155 may be somewhat misleading. Referring to Fig. 23, we see that the predicted attitude on pass 2154 is easily within 0.1° of the 2154 locus. The interaction of the 2154 and 2155 loci however, produces a common area, or attitude box, 1.5° from the pass 2154 prediction. This box is produced by a somewhat grazing intersection of the loci, and its location is therefore affected by the precession which took place between these two passes. Antedating the 2155 locus to account for this would place the attitude box within 0.05° of the 2154 and 2155 prediction, so this fit is quite valid.

We are not in so comfortable a position for passes 3340 and thereafter. Attitude boxes for 3340–1 and 3476–7 are shown as dashed lines on Fig. 23. They are about 20° from the corresponding predicted attitudes, and the reason for this discrepancy is at present unknown. We note that the Telstar I satellite ceased its transmission on pass 2065 (February 20, 1963) because of radiation damage, but that the attitude remained predictable at least through pass 2583. The region from pass 2583 to 3340 is devoid of attitude data because no telemetry could be received to report solar aspect and no mirror flashes were recorded. This was due to the increased activity on Telstar II, a certain proportion of Telstar I passes occurring in daylight hours, and prevailing weather conditions at Holmdel.

Interestingly enough, it is noted that the attitude determinations on passes 3340–1 and 3476–7 can be connected by the magnetic moment program even though they cannot be sensibly joined to the preceding

* It is possible that coil usage can alter the residual moment of the satellite, which was made small in the first place by appropriately balancing much larger magnetic fields.[19]

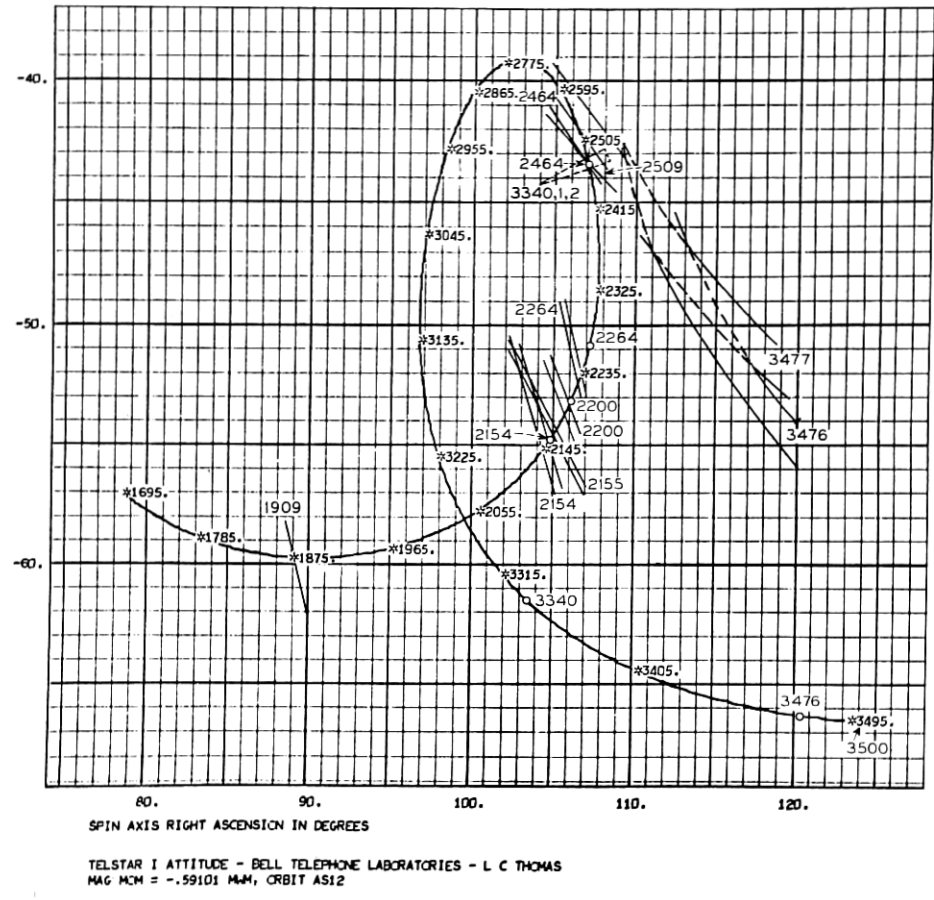

Fig. 23 — Telstar I precessional history — passes 1695 to 3500.

data. Fig. 24 shows this union. The magnetic moment of −0.59101 microweber-meter used in these last three plots cannot be considered too reliable, since it is one of a number which can connect the two attitude boxes shown in Fig. 24. However, it is the same as previously used in the 1695 to 2583 region and may tend to be valid because of this. In any event, more attitude data are required to resolve this issue.

As to what may have caused the anomalous behavior of Telstar I somewhere between pass 2583 and 3440, we offer the following, taken singularly or in combination, as possibilities:

(*i*) the orientation coil has been energized during this period (from

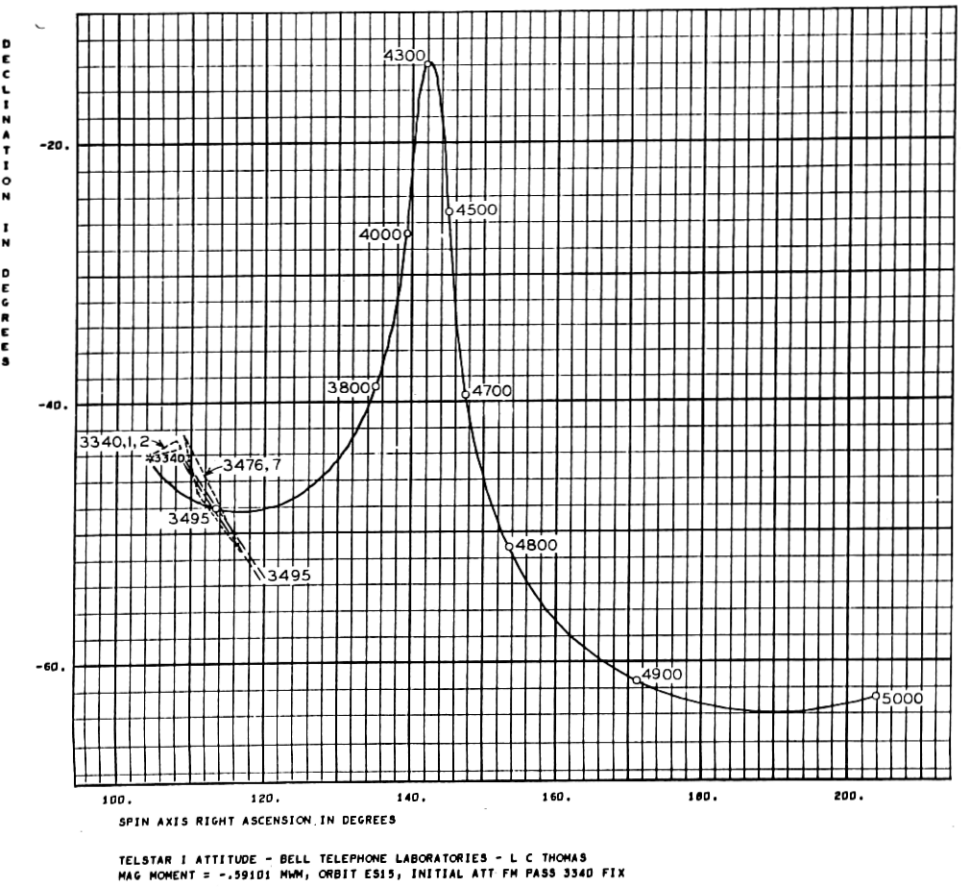

Fig. 24 — Telstar I precessional history and prediction — passes 3340 to 5000.

the present precessional motion, it appears to have been turned off between 3340 and 3477);

(*ii*) the residual magnetic moment has changed a multiplicity of times;

(*iii*) meteoric collision has taken place;

(*iv*) pressure leakage from instrument canister has occurred in a manner to alter the attitude by reaction forces.

5.2 *Experimental Results — The Telstar II Satellite*

The Telstar II satellite entered orbit on May 7, 1963. Its initial attitude calculated from the third-stage burnout parameters is shown

in Table III. The predicted burnout attitude proved inaccurate because the third stage of the Thor-Delta vehicle did not perform nominally. This is evidenced by the fact that the orbital period calculated from such assumed nominal performance differed from the actual period by as much as four minutes.

The first attitude fix of the Telstar II satellite occurred on passes 62 and 63, when a total of three flash series were observed. Connecting this determination to that of pass 496 requires a residual magnetic moment of -0.48375 microweber-meter. The fit through pass 643 is given in Table III, and some typical attitude loci are plotted along with the attitude prediction in Fig. 25. Corresponding ecliptic angle, solar aspect, X and Y torques appear in Figs. 26 through 29.

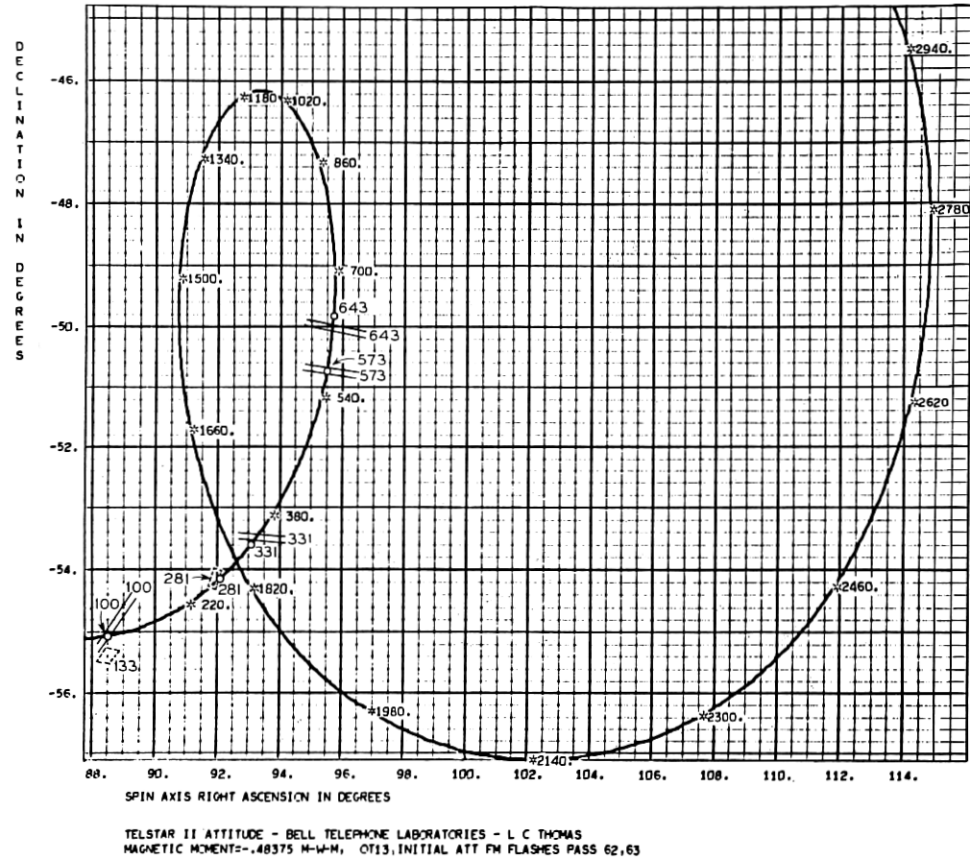

Fig. 25 — Telstar II precessional history and prediction — passes 62 to 3000. (See footnote, p. 1713.)

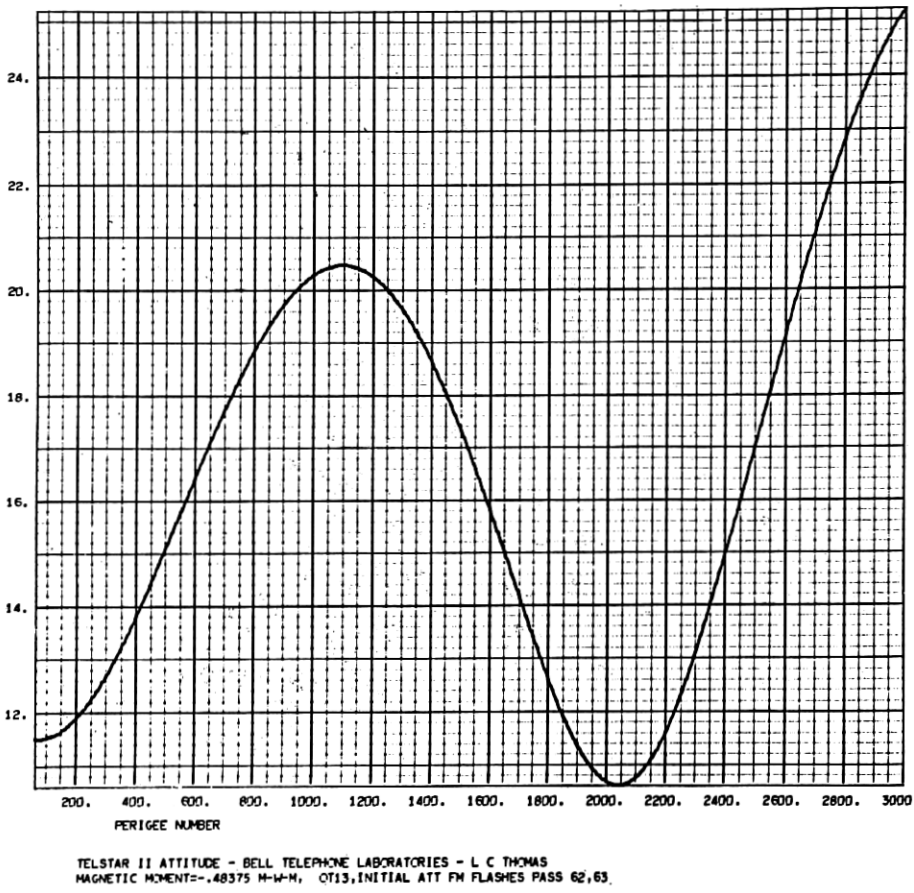

Fig. 26 — Telstar II ecliptic angle — passes 62 to 3000.

The solar offset is due to exceed the 15° limit dictated by temperature balance considerations (see Section I) by pass 1250 (see Fig. 27). Since the maximum offset which occurs on pass 1400 is only 18°, no plans are contemplated to reorient the Telstar II satellite strictly to prevent this mild excursion.

There is, however, another excursion beyond the 15° limit, around pass 2670. Besides this excursion being more serious than the former, some interesting differences between these two events exist, as Fig. 25 illustrates.

On pass 1400, the attitude will be returning to a region nearer the south ecliptic pole (located at right ascension 90°, declination 67.5°)

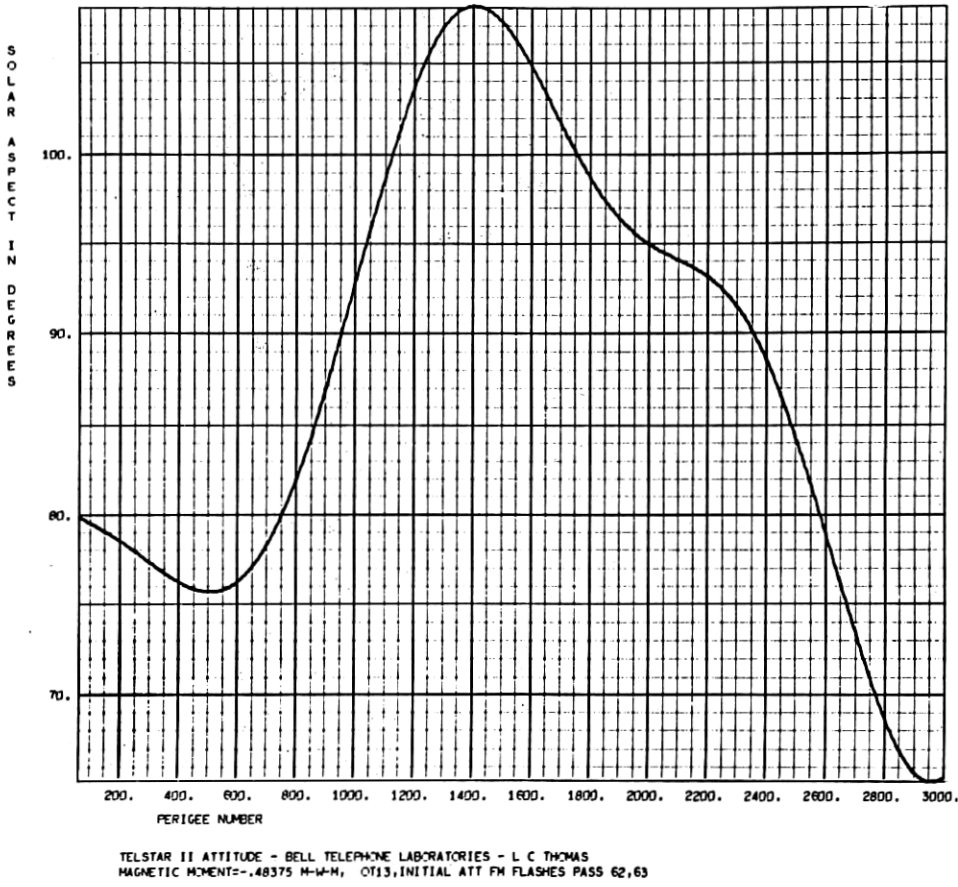

Fig. 27 — Telstar II solar aspect — passes 62 to 3000.

thereby limiting the solar offset to values below 15°. On pass 2670, however, the attitude is moving away from the south ecliptic pole, and, in fact, because of its now lower spin rate is entering a spiral of greater excursion than that previously traversed. It therefore behooves us to correct the attitude before that latter spiral occurs.

The question remaining is to determine the most profitable time for such a correction. Ideally, a well-chosen time would meet the following conditions:

(*i*) It would take place just after a good optical attitude fix was established to verify the predictions.

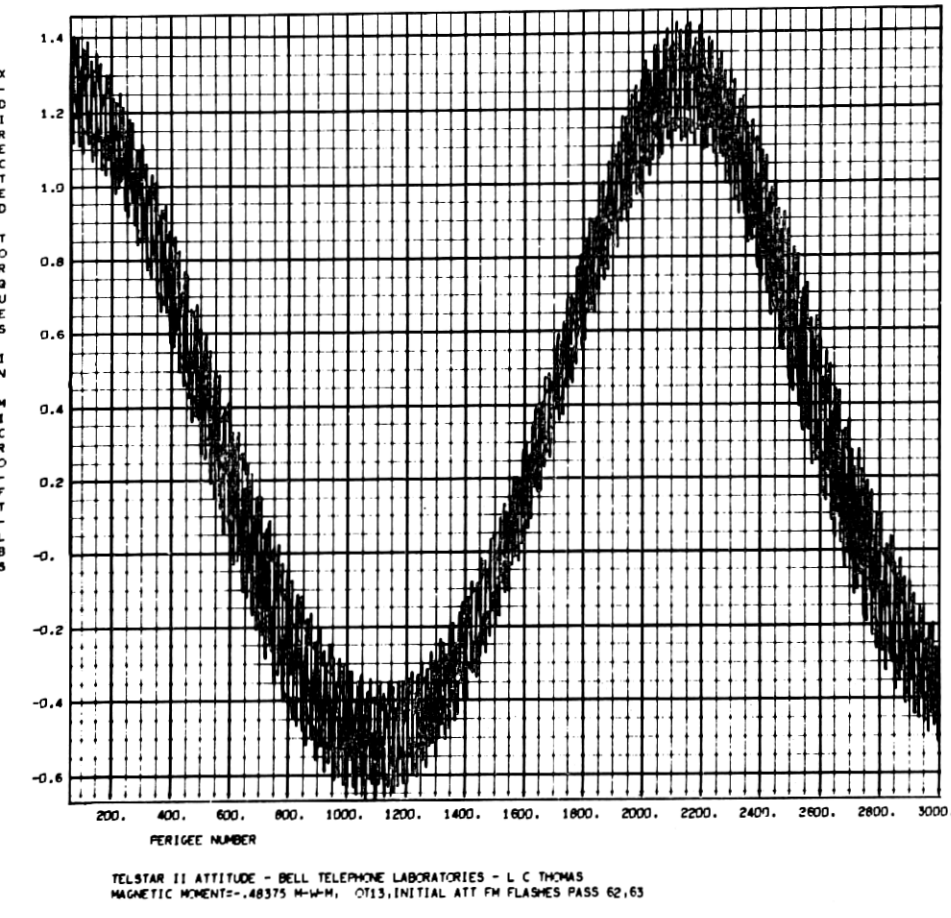

Fig. 28 — Telstar II X torques — passes 62 to 3000.

(*ii*) The attitude maneuver would result in as many mirror flashes as possible during correction to indicate its progress.

(*iii*) The attitude maneuver would end with the satellite in a position to guarantee a suitable attitude for as long a time in the future as is possible.

At the time of this writing, suitable attitude corrections are under study. Most probably the orientation coil will be energized sometime between passes 1300 to 1500 in a negative sense or in a positive sense near pass 2400 so as to drive the attitude downward and to the left in

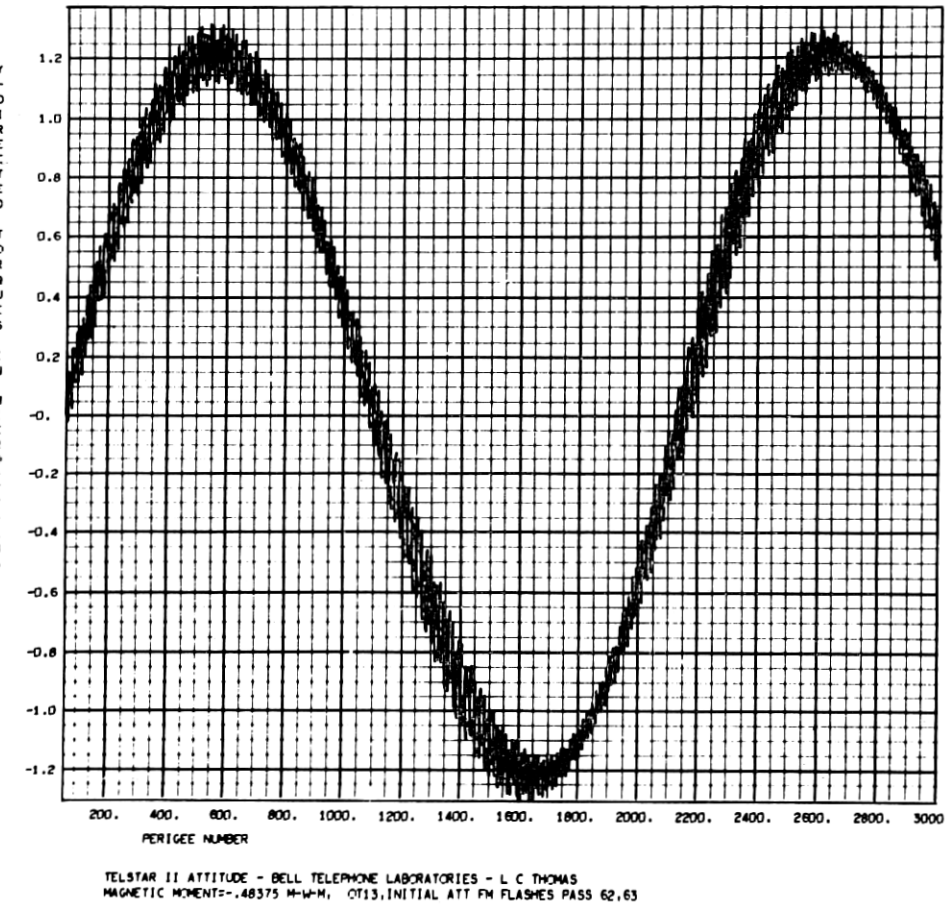

Fig. 29 — Telstar II Y torques — passes 62 to 3000.

the sense shown in Fig. 25. This permits the next attitude spiral to occur near the south ecliptic pole.*

VI. CONCLUSIONS

Techniques for both attitude determination and prediction for spin-stabilized satellites have been developed. Their use has been demon-

* The attitude of the Telstar II satellite was successfully reoriented by energizing the coil on pass 2402 (May 17, 1964) and leaving it in that state until pass 2421. Thus attitude predictions given in Fig. 19 beyond pass 2402 are no longer valid.

strated using Telstar I and II satellite data. It has been shown that an inclined dipole model of the earth's magnetic field and the method of averaging the gravitational and magnetic torques over each anomalistic period of the satellite permit attitude predictions to within a few tenths of a degree of determined values in most instances. In those few cases where departures are above one degree, explanations have been presented to show the reason for such discrepancies. The reasons are (1) unknown time errors in determining the midpoint of the optical flash series and (2) grazing intersections of the attitude determining loci. There remains but one anomaly in the precessional motion of the Telstar I satellite which, for the moment, is unexplained. Possible reasons for this anomaly are given in Section 5.1.

It has further been shown that the seemingly crude approximation of letting the mean anomaly of the satellite equal the true anomaly for the purposes of determining the mean torques produces attitudes in close agreement (0.01° over 1000 orbits) with more sophisticated approximations for orbit eccentricities up to 0.9 and perigee radii above about 4500 miles. (See Section 4.6, case II.)

The comparisons made herein of the precession given by the magnetic moment program and the attitude determinations substantiate the simplifying assumptions made in Sections 4.1, 4.2, and 4.3. These assumptions are most instrumental in producing a working technique for both attitude prediction and residual magnetic moment determination which is amenable to analytic solution and conservative of computer time.

Furthermore, the usefulness of combining optical flash and solar sensor data for attitude determination and their inherent accuracy is shown. Optical flash data can provide loci with a resolution of 0.1°. Solar sensor loci are resolved to within 1°. While it is clearly straightforward to determine analytically the boundaries of the attitude boxes from intersecting loci exhibiting estimated time tolerances, this paper indicates the decided advantage of graphing the individual loci to determine the angle of intersection and thereby gain an estimate of the validity of the boundaries in the presence of precession (see, for example, Section 4.1).

Finally, the techniques described have all been consolidated into working computer programs which follow closely the analysis presented. In addition, a number of important supporting calculations such as the solar position, sidereal time, orbit updating, etc. are developed. Because of the complexities of the mean torque and gyroscopic equations, the precessional analysis is most useful when embodied in suitable computer programs.

VII. ACKNOWLEDGMENTS

The author acknowledges his indebtedness to the following contributors as indicated: to J. F. Ossanna for orbital updating techniques specifically, and in general for helpful discussions concerning computer techniques useful for the calculations; to J. S. Courtney-Pratt, J. W. McLaughlin, and J. H. Hett for the development of techniques and equipment to record the optical flashes at the Holmdel Laboratories, and for their splendid cooperation throughout this project; to W. C. Jakes, Jr., L. R. Lowry, W. E. Legg, R. H. Brandt, P. E. Pheffer, J. W. Barto, and E. L. Frantsvog for providing and staffing Holmdel facilities to acquire and track the Telstar satellites and for useful work in ascertaining the attitude from antenna pattern measurements; to D. W. Hill for initially developing the concept of reducing attitude from mirror flashes and solar sensor data; to R. C. Chapman for patiently reading, correcting and rendering advice on this manuscript; to R. H. Shennum for close cooperation, advice and aid during the period of attitude correction; and to I. Welber for helpful integration of this work into the Telstar satellite communications experiment.

APPENDIX A

Derivation of Equation (40)[21]

Beginning with (39) of the main body of the paper, it is certainly evident that

$$\mathbf{k}\cdot(\mathbf{i}_g\mathbf{i}_g + \mathbf{j}_g\mathbf{j}_g) \times \mathbf{k} = (\mathbf{k}\cdot\mathbf{i}_g)(\mathbf{i}_g \times \mathbf{k}) + (\mathbf{k}\cdot\mathbf{j}_g)(\mathbf{j}_g \times \mathbf{k}). \quad (39a)$$

It will be shown that the following identity exists

$$(\mathbf{k}\cdot\mathbf{i}_g)(\mathbf{i}_g \times \mathbf{k}) + (\mathbf{k}\cdot\mathbf{j}_g)(\mathbf{j}_g \times \mathbf{k}) + (\mathbf{k}\cdot\mathbf{k}_g)(\mathbf{k}_g \times \mathbf{k}) \equiv 0. \quad (39b)$$

Rewriting (39b), one obtains

$$[(\mathbf{k}\cdot\mathbf{i}_g)\mathbf{i}_g + (\mathbf{k}\cdot\mathbf{j}_g)\mathbf{j}_g + (\mathbf{k}\cdot\mathbf{k}_g)\mathbf{k}_g] \times \mathbf{k} \equiv 0 \quad (39c)$$

and

$$(\mathbf{k}\cdot\mathbf{i}_g) = (x_g\mathbf{i}_g + y_g\mathbf{j}_g + z_g\mathbf{k}_g)\cdot\mathbf{i}_g \quad (39d)$$

$$= x_g \quad (39e)$$

where

x_g , y_g , z_g = components of $\mathbf{k}$ along the ORDEF axes.

In like fashion

$$(\mathbf{k}\cdot\mathbf{j}_g) = y_g \tag{39f}$$

$$(\mathbf{k}\cdot\mathbf{k}_g) = z_g\,. \tag{39g}$$

Substituting (39e,f,g) into (39c), we obtain

$$(x_g\mathbf{i}_g + y_g\mathbf{j}_g + z_g\mathbf{k}_g) \times \mathbf{k} \equiv 0 \tag{39h}$$

$$\mathbf{k} \times \mathbf{k} = 0 \tag{39i}$$

$$0 \equiv 0. \tag{39j}$$

Therefore

$$-(\mathbf{k}\cdot\mathbf{k}_g)(\mathbf{k}_g \times \mathbf{k}) \equiv \mathbf{k}\cdot(\mathbf{i}_g\mathbf{i}_g + \mathbf{j}_g\mathbf{j}_g) \times \mathbf{k}, \tag{39k}$$

and (40) follows from (39).

APPENDIX B

Evaluation of the II Integral of Equation (73)[21]

Copying the II integral from (73) of the main body of the paper, we have

$$\text{II} = (\cos\beta)\mathbf{k} \times \int_0^{2\pi} \{\mathbf{K} - 3(\mathbf{i}_s\cdot\mathbf{K})\mathbf{i}_s\}\,(1 + e\cos v)\,dv\,. \tag{74}$$

Split (74) into two parts by letting

$$\begin{aligned}\text{IIA} &= \cos\beta\mathbf{k} \times \mathbf{K} \int_0^{2\pi} (1 + \cos v)\,dv \\ &= \cos\beta\mathbf{K} \times \int_0^{2\pi} (1 + e\cos\omega\cos P + e\sin\omega\sin P)\,d\omega \\ &= (2\pi\cos\beta)\mathbf{k} \times \mathbf{K}\end{aligned} \tag{75}$$

and

$$\begin{aligned}\text{IIB} = (-3\cos\beta)\mathbf{k} \times \mathbf{K}\cdot \int_0^{2\pi} \mathbf{i}_s\mathbf{i}_s(1 + e\cos\omega\cos P \\ + e\sin\omega\sin P)\,d\omega\,.\end{aligned} \tag{76}$$

But

$$\mathbf{i}_s = \cos\omega\mathbf{i}_g + \sin\omega\mathbf{j}_g \tag{77}$$

therefore

$$\mathbf{i}_s\mathbf{i}_s = \cos^2 \omega\mathbf{i}_v\mathbf{i}_v + \sin^2 \omega\mathbf{j}_v\mathbf{j}_v + \sin \omega \cos \omega(\mathbf{i}_v\mathbf{j}_v + \mathbf{j}_v\mathbf{i}_v). \tag{78}$$

It follows that

$$\text{IIB} = (-3\pi \cos\beta)\mathbf{k} \times \mathbf{K} \cdot (\mathbf{i}_v\mathbf{i}_v + \mathbf{j}_v\mathbf{j}_v). \tag{79}$$

So that, combining IIA and IIB

$$\text{II} = (\pi \cos\beta)\mathbf{k} \times [2\mathbf{K} - 3\mathbf{K} \cdot (\mathbf{i}_v\mathbf{i}_v + \mathbf{j}_v\mathbf{j}_v)] \tag{80}$$

$$= (\pi \cos\beta)\mathbf{k} \times [2\mathbf{K} - 3(\mathbf{K} \cdot \mathbf{j}_v)\mathbf{j}_v] \tag{81}$$

$$= \pi \cos\beta[2\mathbf{k} \times \mathbf{K} - 3(\mathbf{K} \cdot \mathbf{j}_v)(\mathbf{k}X\mathbf{j}_v)]. \tag{82}$$

We shall now proceed to express (82) in the SANOR system. From Fig. 10,

$$\mathbf{K} = \sin\theta\mathbf{j} + \cos\theta\mathbf{k}. \tag{83}$$

From (22) and (20) we write

$$x_v = (CD)_i(\tilde{D}\tilde{C})x \tag{84}$$

or

$$\begin{aligned}\mathbf{j}_v = {} & (\sin\psi \cos\Omega \cos i - \sin\Omega \cos\psi \cos i)\mathbf{i} \\ & + (\sin i \sin\theta + \sin\Omega \cos i \sin\psi \cos\theta \\ & + \cos\Omega \cos i \cos\psi \cos\theta)\mathbf{j} \\ & + (\sin i \cos\theta - \sin\Omega \cos i \sin\psi \sin\theta \\ & - \cos\Omega \cos i \cos\psi \sin\theta)\mathbf{k}\end{aligned} \tag{85}$$

or, simplifying

$$\begin{aligned}\mathbf{j}_v = {} & [-\cos i \sin(\Omega - \psi)]\mathbf{i} \\ & + [\sin i \sin\theta + \cos i \cos\theta \cos(\Omega - \psi)]\mathbf{j} \\ & + [\sin i \cos\theta - \cos i \sin\theta \cos(\Omega - \psi)]\mathbf{k}.\end{aligned} \tag{86}$$

Substitute (83) and (86) into (82) to obtain

$$\begin{aligned}\text{II} = {} & \pi \cos\beta\Big[(-2 \sin\theta)\mathbf{i} - 3[\{\sin i \sin^2\theta \\ & + \cos i \sin\theta \cos\theta \cos(\Omega - \psi) + \sin i \cos^2\theta \\ & - \cos i \sin\theta \cos\theta \cos(\Omega - \psi)\}\{(-\sin i \sin\theta \\ & - \cos i \cos\theta \cos(\Omega - \psi))\mathbf{i} \\ & + (-\cos i \sin(\Omega - \psi))\mathbf{j}\}]\Big].\end{aligned} \tag{87}$$

Finally,

$$\begin{aligned}\text{II} = \pi \cos\beta[\{&-2\sin\theta + 3\sin^2 i \sin\theta \\ &+ 3\sin i \cos i \cos\theta \cos(\Omega - \psi)\}\mathbf{i} \\ &+ 3\sin i \cos i \sin(\Omega - \psi)\mathbf{j}].\end{aligned} \tag{88}$$

APPENDIX C

Case I Expansion

Refer to integrals of (91), (92), (93), and (94) of the main body of the paper:

$$A = \int_0^{2\pi} \sin\eta_0(1 + e\cos v)\,dv = \int_0^{2\pi} \sin\eta_0\,dv + e\int_0^{2\pi} \sin\eta_0 \cos v\,dv \tag{109}$$

$$\begin{aligned}&= \sin\eta_0 \int_0^{2\pi} \cos(bv)\,dv + \cos\eta_0 \int_0^{2\pi} \sin(bv)\,dv \\ &\quad + e\left[\sin\eta_0 \int_0^{2\pi} \cos(bv)\cos v\,dv\right. \\ &\quad \left. + \cos\eta_0 \int_0^{2\pi} \sin(bv)\cos v\,dv\right]\end{aligned} \tag{110}$$

$$= \sin\eta_0(D_1 + eD_3) + \cos\eta_0(D_2 + eD_4) \tag{111}$$

$$= \left(\frac{1}{b} - \frac{eb}{1 - b^2}\right)[\sin\eta_0 \sin 2\pi b + \cos\eta_0(1 - \cos 2\pi b)] \tag{112}$$

where the D factors are listed in Appendix E. In similar manner,

$$B = \cos\eta_0(D_1 + eD_3) - \sin\eta_0(D_2 + eD_4) \tag{113}$$

$$= \left[\frac{1}{b} - \frac{eb}{1 - b^2}\right][\cos\eta_0 \sin 2\pi b - \sin\eta_0(1 - \cos 2\pi b)]. \tag{114}$$

The **C** integral is expanded as follows

$$\mathbf{C} = \int_0^{2\pi} \mathbf{i}_s\mathbf{i}_s \sin\eta(1 + e\cos v)\,dv \tag{115}$$

but

$$\mathbf{i}_s = \cos\omega\mathbf{i}_g + \sin\omega\mathbf{j}_g\,. \tag{116}$$

Therefore

$$\mathbf{i}_s\mathbf{i}_s = \cos^2 \omega \mathbf{i}_\theta\mathbf{i}_\theta + \sin^2 \omega \mathbf{j}_\theta\mathbf{j}_\theta + \sin \omega \cos \omega(\mathbf{i}_\theta\mathbf{j}_\theta + \mathbf{j}_\theta\mathbf{i}_\theta). \quad (117)$$

Let

$$\mathbf{C} = \mathbf{i}_\theta\mathbf{i}_\theta C_1 + \mathbf{j}_\theta\mathbf{j}_\theta C_2 + (\mathbf{i}_\theta\mathbf{j}_\theta + \mathbf{j}_\theta\mathbf{i}_\theta)C_3 \quad (118)$$

and evaluate C_1, C_2, C_3 separately.

$$C_1 = \int_0^{2\pi} \cos^2 \omega \sin \eta(1 + e \cos v)\, dv. \quad (119)$$

Letting $\omega = v + P$, expanding $\cos^2 \omega$ and collecting terms, we have

$$\begin{aligned} C_1 = \sin \eta_0[&\cos^2 P(D_5 + eD_7) + \sin^2 P(D_9 + eD_{11}) \\ &- 2 \sin P \cos P(D_{13} + eD_{15})] \\ + \cos \eta_0[&\cos^2 P(D_6 + eD_8) + \sin^2 P(D_{10} + eD_{12}) \\ &- 2 \sin P \cos P(D_{14} + eD_{16})]. \end{aligned} \quad (120)$$

in like fashion

$$\begin{aligned} C_2 = \sin \eta_0[&\sin^2 P(D_5 + eD_7) + \cos^2 P(D_9 + eD_{11}) \\ &+ 2 \sin P \cos P(D_{13} + eD_{15})] \\ + \cos \eta_0[&\sin^2 P(D_6 + eD_8) + \cos^2 P(D_{10} + eD_{12}) \\ &+ 2 \sin P \cos P(D_{14} + eD_{16})] \end{aligned} \quad (121)$$

and

$$\begin{aligned} C_3 &= \int_0^{2\pi} \sin \omega \cos \omega \sin \eta(1 + e \cos v)\, dv \\ &= \sin \eta_0[(\cos^2 P - \sin^2 P)(D_{13} + eD_{15}) \\ &\quad + \sin P \cos P\,(D_5 - D_9 + eD_7 - eD_{11})] \\ &\quad + \cos \eta_0[(\cos^2 P - \sin^2 P)(D_{14} + eD_{16}) \\ &\quad + \sin P \cos P\,(D_6 - D_{10} + eD_8 - eD_{12})]. \end{aligned} \quad (122)$$

Since

$$\mathbf{E} = \int_0^{2\pi} \mathbf{i}_s\mathbf{i}_s \cos \eta(1 + e \cos v)\, dv \quad (94)$$

we expand as with $\mathbf{C}$, to yield

$$\mathbf{E} = \mathbf{i}_\theta\mathbf{i}_\theta E_1 + \mathbf{j}_\theta\mathbf{j}_\theta E_2 + (\mathbf{i}_\theta\mathbf{j}_\theta + \mathbf{j}_\theta\mathbf{i}_\theta)E_3 \quad (123)$$

so that

$$E_1 = \int_0^{2\pi} \cos^2 \omega \cos \eta(1 + e \cos v)\, dv \tag{124}$$

$$\begin{aligned} &= \cos \eta_0[\cos^2 P(D_5 + eD_7) + \sin^2 P(D_9 + eD_{11}) \\ &\quad - 2 \sin P \cos P(D_{13} + eD_{15})] \\ &\quad - \sin \eta_0[\cos^2 P(D_6 + eD_8) + \sin^2 P(D_{10} + eD_{12}) \\ &\quad - 2 \sin P \cos P(D_{14} + eD_{16})] \end{aligned} \tag{125}$$

and

$$E_2 = \int_0^{2\pi} \sin^2 \omega \cos \eta(1 + e \cos v)\, dv$$

$$\begin{aligned} &= \cos \eta_0[\sin^2 P(D_5 + eD_7) + \cos^2 P(D_9 + eD_{11}) \\ &\quad + 2 \sin P \cos P(D_{13} + eD_{15})] \\ &\quad - \sin \eta_0[\sin^2 P(D_6 + eD_8) + \cos^2 P(D_{10} + eD_{12}) \\ &\quad + 2 \sin P \cos P(D_{14} + eD_{16})] \end{aligned} \tag{127}$$

and

$$E_3 = \int_0^{2\pi} \sin \omega \cos \omega \cos \eta(1 + e \cos v)\, dv \tag{128}$$

$$\begin{aligned} &= \cos \eta_0[(\cos^2 P - \sin^2 P)(D_{13} + eD_{15}) \\ &\quad + \sin P \cos P(D_5 - D_9 + eD_7 - eD_{11})] \\ &\quad - \sin \eta_0[(\cos^2 P - \sin^2 P)(D_{14} + eD_{16}) \\ &\quad + \sin P \cos P(D_6 - D_{10} + eD_8 - eD_{12})]. \end{aligned} \tag{129}$$

APPENDIX D

Case II Expansion

We will now evaluate (91), (92), (93) and (94) once again in a manner similar to Appendix C, but this time using the approximation

$$M = v - (\lambda/b) \sin v. \tag{102}$$

The same notation will be used for the integrals

$$A = \int_0^{2\pi} \sin \eta(1 + e \cos v)\, dv$$

$$\begin{aligned} = \sin \eta_0 \int_0^{2\pi} &\{\cos bv \cos (\lambda \sin v) + \sin bv \sin (\lambda \sin v)\} \\ &\cdot (1 + e \cos v)\, dv \\ + \cos \eta_0 \int_0^{2\pi} &\{\sin bv \cos (\lambda \sin v) - \cos bv \sin (\lambda \sin v)\} \\ &\cdot (1 + e \cos v)\, dv. \end{aligned} \tag{143}$$

Using the approximations of (107) and (108), we have

$$\begin{aligned} A = \sin \eta_0 &[D_1 + eD_3 + \lambda(D_{17} + eD_{14}) - (\lambda^2/2)(D_9 + eD_{11}) \\ &- (\lambda^3/6)(D_{18} + eD_{19})] \\ + \cos \eta_0 &[D_2 + eD_4 - \lambda(D_{20} + eD_{13}) - (\lambda^2/2) \\ &(D_{10} + eD_{12}) + (\lambda^3/6)(D_{21} + eD_{22})]. \end{aligned} \tag{144}$$

In like manner,

$$B = \int_0^{2\pi} \cos \eta(1 + e \cos v)\, dv \tag{145}$$

$$\begin{aligned} = \cos \eta_0 &[D_1 + eD_3 + \lambda(D_{17} + eD_{14}) - (\lambda^2/2)(D_9 + eD_{11}) \\ &- (\lambda^3/6)(D_{18} + eD_{19})] \\ - \sin \eta_0 &[D_2 + eD_4 - \lambda(D_{20} + eD_{13}) - (\lambda^2/2)(D_{10} \\ &+ eD_{12}) + (\lambda^3/6)(D_{21} + eD_{22})]. \end{aligned} \tag{146}$$

Similarly,

$$C_1 = \int_0^{2\pi} \cos^2 \omega \sin \eta(1 + e \cos v)\, dv \tag{147}$$

$$\begin{aligned} C_1 = \sin \eta_0 \Big[&\cos^2 P\{(D_5 + eD_7) + \lambda(D_{16} + eD_{26}) - (\lambda^2/2)(D_{23} \\ &+ eD_{25}) - (\lambda^3/6)(D_{31} + eD_{33})\} + \sin^2 P\{(D_9 + eD_{11}) \\ &+ \lambda(D_{18} + eD_{19}) - (\lambda^2/2)(D_{30} + eD_{38}) - (\lambda^3/6) \\ &\cdot (D_{35} + eD_{41})\} - 2 \sin P \cos P\{(D_{13} + eD_{15}) + \lambda(D_{12} \end{aligned}$$

$$+ eD_{24}) - (\lambda^2/2)(D_{22} + eD_{32}) - (\lambda^3/6)(D_{37} + eD_{39})\}\Big] + \cos \eta_0\Big[\cos^2 P\{(D_6 + eD_8) - \lambda(D_{15} + eD_{28}) - (\lambda^2/2) \cdot (D_{24} + eD_{27}) + (\lambda^3/6)(D_{32} + eD_{34})\} + \sin^2 P\{(D_{10} + eD_{12}) - \lambda(D_{21} + eD_{22}) - (\lambda^2/2)(D_{29} + eD_{37}) + (\lambda^3/6)(D_{36} + eD_{42})\} - 2 \sin P \cos P\{(D_{14} + eD_{16}) - \lambda(D_{11} + eD_{23}) - (\lambda^2/2)(D_{19} + eD_{31}) + (\lambda^3/6)(D_{38} + eD_{40})\}\Big]. \tag{148}$$

To simplify the writing of the mean magnetic torque equation, let

$$F_1 = (D_5 + eD_7) + \lambda(D_{16} + eD_{26}) - (\lambda^2/2)(D_{23} + eD_{25}) - (\lambda^3/6)(D_{31} + eD_{33}) \tag{122}$$

$$F_2 = (D_9 + eD_{11}) + \lambda(D_{18} + eD_{19}) - (\lambda^2/2)(D_{30} + eD_{38}) - (\lambda^3/6)(D_{35} + eD_{41}) \tag{123}$$

$$F_3 = (D_{13} + eD_{15}) + \lambda(D_{12} + eD_{24}) - (\lambda^2/2)(D_{22} + eD_{32}) - (\lambda^3/6)(D_{36} + eD_{39}) \tag{124}$$

$$F_4 = (D_6 + eD_8) - \lambda(D_{15} + eD_{28}) - (\lambda^2/2)(D_{24} + eD_{27}) + (\lambda^3/6)(D_{32} + eD_{34}) \tag{125}$$

$$F_5 = (D_{10} + eD_{12}) - \lambda(D_{21} + eD_{22}) - (\lambda^2/2)(D_{29} + eD_{37}) + (\lambda^3/6)(D_{36} + eD_{42}) \tag{126}$$

$$F_6 = (D_{14} + eD_{16}) - \lambda(D_{11} + eD_{23}) - (\lambda^2/2)(D_{19} + eD_{31}) + (\lambda^3/6)(D_{38} + eD_{40}). \tag{127}$$

By the similarity of C_2 and C_3 integrals to C_1 and of E_1, E_2, E_3 to C_1, C_2, C_3 we immediately write and summarize the following:

$$C_1 = \sin \eta_0[F_1 \cos^2 P + F_2 \sin^2 P - 2F_3 \sin P \cos P] + \cos \eta_0[F_4 \cos^2 P + F_5 \sin^2 P - 2F_6 \sin P \cos P] \tag{128}$$

$$C_2 = \sin \eta_0[F_1 \sin^2 P + F_2 \cos^2 P + 2F_3 \sin P \cos P] + \cos \eta_0[F_4 \sin^2 P + F_5 \cos^2 P + 2F_6 \sin P \cos P] \tag{129}$$

$$C_3 = \sin \eta_0[(F_1 - F_2) \sin P \cos P + F_3(\cos^2 P - \sin^2 P)] + \cos \eta_0[(F_4 - F_5) \sin P \cos P + F_6(\cos^2 P - \sin^2 P)] \tag{130}$$

$$E_1 = \cos \eta_0[F_1 \cos^2 P + F_2 \sin^2 P - 2F_3 \sin P \cos P] - \sin \eta_0[F_4 \cos^2 P + F_5 \sin^2 P - 2F_6 \sin P \cos P] \tag{131}$$

$$E_2 = \cos \eta_0[F_1 \sin^2 P + F_2 \cos^2 P + 2F_3 \sin P \cos P] - \sin \eta_0[F_4 \sin^2 P + F_5 \cos^2 P + 2F_6 \sin P \cos P] \tag{132}$$

$$E_3 = \cos \eta_0[(F_1 - F_2) \sin P \cos P + F_3(\cos^2 P - \sin^2 P)] - \sin \eta_0[(F_4 - F_5) \sin P \cos P + F_6(\cos^2 P - \sin^2 P)]. \tag{133}$$

APPENDIX E

The D Integrals[22]

$$D_1 = \int_0^{2\pi} \cos (bv)\, dv = \frac{1}{b} \sin (2\pi b)$$

$$D_2 = \int_0^{2\pi} \sin (bv)\, dv = \frac{1}{b} [1 - \cos (2\pi b)]$$

$$D_3 = \int_0^{2\pi} \cos (bv) \cos v\, dv = -\frac{b \sin (2\pi b)}{1 - b^2}$$

$$D_4 = \int_0^{2\pi} \sin (bv) \cos v\, dv = -\frac{b}{1 - b^2} [1 - \cos (2\pi b)]$$

$$D_5 = \int_0^{2\pi} \cos (bv) \cos^2 v\, dv = \frac{2 - b^2}{b(4 - b^2)} \sin (2\pi b)$$

$$D_6 = \int_0^{2\pi} \sin (bv) \cos^2 v\, dv = \frac{2 - b^2}{b(4 - b^2)} [1 - \cos (2\pi b)]$$

$$D_7 = \int_0^{2\pi} \cos (bv) \cos^3 v\, dv = -\frac{b(7 - b)^2}{(1 - b^2)(9 - b^2)} \sin (2\pi b)$$

$$D_8 = \int_0^{2\pi} \sin (bv) \cos^3 v\, dv = -\frac{b(7 - b^2)}{(1 - b^2)(9 - b^2)} [1 - \cos (2\pi b)]$$

$$D_9 = \int_0^{2\pi} \cos (bv) \sin^2 v\, dv = \frac{2 \sin (2\pi b)}{b(4 - b^2)}$$

$$D_{10} = \int_0^{2\pi} \sin (bv) \sin^2 v\, dv = \frac{2}{b(4 - b^2)} [1 - \cos (2\pi b)]$$

$$D_{11} = \int_0^{2\pi} \sin^2 v \cos v \cos (bv)\, dv = -\frac{2b \sin (2\pi b)}{(1 - b^2)(9 - b^2)}$$

$$D_{12} = \int_0^{2\pi} \sin^2 v \cos v \sin (bv)\, dv = \frac{-2b}{(1 - b^2)(9 - b^2)} [1 - \cos (2\pi b)]$$

$$D_{13} = \int_0^{2\pi} \sin v \cos v \cos (bv)\, dv = \frac{1 - \cos (2\pi b)}{4 - b^2}$$

$$D_{14} = \int_0^{2\pi} \sin v \cos v \sin (bv)\, dv = -\frac{\sin (2\pi b)}{4 - b^2}$$

$$D_{15} = \int_0^{2\pi} \sin v \cos^2 v \cos (bv)\, dv = \frac{(3 - b^2)}{(9 - b^2)(1 - b^2)} [1 - \cos (2\pi b)]$$

$$D_{16} = \int_0^{2\pi} \sin v \cos^2 v \sin (bv)\, dv = -\frac{(3 - b^2) \sin (2\pi b)}{(9 - b^2)(1 - b^2)}$$

$$D_{17} = \int_0^{2\pi} \sin v \sin (bv)\, dv = -\frac{\sin (2\pi b)}{1 - b^2}$$

$$D_{18} = \int_0^{2\pi} \sin^3 v \sin (bv)\, dv = -\frac{6 \sin (2\pi b)}{(9 - b^2)(1 - b^2)}$$

$$D_{19} = \int_0^{2\pi} \sin^3 v \cos v \sin (bv)\, dv = -\frac{6 \sin (2\pi b)}{(16 - b^2)(4 - b^2)}$$

$$D_{20} = \int_0^{2\pi} \sin v \cos (bv)\, dv = \frac{1 - \cos (2\pi b)}{1 - b^2}$$

$$D_{21} = \int_0^{2\pi} \sin^3 v \cos (bv)\, dv = \frac{6[1 - \cos (2\pi b)]}{(9 - b^2)(1 - b^2)}$$

$$D_{22} = \int_0^{2\pi} \sin^3 v \cos v \cos (bv)\, dv = \frac{6[1 - \cos (2\pi b)]}{(16 - b^2)(4 - b^2)}$$

$$D_{23} = \int_0^{2\pi} \sin^2 v \cos^2 v \cos (bv)\, dv = \frac{2 \sin (2\pi b)}{b(16 - b^2)}$$

$$D_{24} = \int_0^{2\pi} \sin^2 v \cos^2 v \sin (bv)\, dv = \frac{2[1 - \cos (2\pi b)]}{b(16 - b^2)}$$

$$D_{25} = \int_0^{2\pi} \sin^2 v \cos^3 v \cos (bv)\, dv = -\frac{2b(13 - b^2) \sin (2\pi b)}{(25 - b^2)(9 - b^2)(1 - b^2)}$$

$$D_{26} = \int_0^{2\pi} \sin v \cos^3 v \sin (bv)\, dv = -\frac{(10 - b^2) \sin (2\pi b)}{(16 - b^2)(4 - b^2)}$$

$$D_{27} = \int_0^{2\pi} \sin^2 v \cos^3 v \sin (bv)\, dv = -\frac{2b(13 - b^2)[1 - \cos (2\pi b)]}{(25 - b^2)(9 - b^2)(1 - b^2)}$$

$$D_{28} = \int_0^{2\pi} \sin v \cos^3 v \cos (bv)\, dv = \frac{(10 - b^2)[1 - \cos (2\pi b)]}{(16 - b^2)(4 - b^2)}$$

$$D_{29} = \int_0^{2\pi} \sin^4 v \sin (bv)\, dv = \frac{24[1 - \cos (2\pi b)]}{b(16 - b^2)(4 - b^2)}$$

$$D_{30} = \int_0^{2\pi} \sin^4 v \cos (bv)\, dv = \frac{24 \sin (2\pi b)}{b(16 - b^2)(4 - b^2)}$$

$$D_{31} = \int_0^{2\pi} \sin^3 v \cos^2 v \sin (bv)\, dv = -\frac{6(5 - b^2) \sin (2\pi b)}{(25 - b^2)(9 - b^2)(1 - b^2)}$$

$$D_{32} = \int_0^{2\pi} \sin^3 v \cos^2 v \cos (bv)\, dv = \frac{6(5 - b^2)[1 - \cos (2\pi b)]}{(25 - b^2)(9 - b^2)(1 - b^2)}$$

$$D_{33} = \int_0^{2\pi} \sin^3 v \cos^3 v \sin (bv)\, dv = -\frac{6 \sin (2\pi b)}{(36 - b^2)(4 - b^2)}$$

$$D_{34} = \int_0^{2\pi} \sin^3 v \cos^3 v \cos (bv)\, dv = \frac{6[1 - \cos (2\pi b)]}{(36 - b^2)(4 - b^2)}$$

$$D_{35} = \int_0^{2\pi} \sin^5 v \sin (bv)\, dv = -\frac{120 \sin (2\pi b)}{(25 - b^2)(9 - b^2)(1 - b^2)}$$

$$D_{36} = \int_0^{2\pi} \sin^5 v \cos (bv)\, dv = \frac{120[1 - \cos (2\pi b)]}{(25 - b^2)(9 - b^2)(1 - b^2)}$$

$$D_{37} = \int_0^{2\pi} \sin^4 v \cos v \sin (bv)\, dv = -\frac{24b[1 - \cos (2\pi b)]}{(25 - b^2)(9 - b^2)(1 - b^2)}$$

$$D_{38} = \int_0^{2\pi} \sin^4 v \cos v \cos (bv)\, dv = -\frac{24b \sin (2\pi b)}{(25 - b^2)(9 - b^2)(1 - b^2)}$$

$$D_{39} = \int_0^{2\pi} \sin^4 v \cos^2 v \sin (bv)\, dv = \frac{24(6 - b^2)[1 - \cos (2\pi b)]}{b(36 - b^2)(16 - b^2)(4 - b^2)}$$

$$D_{40} = \int_0^{2\pi} \sin^4 v \cos^2 v \cos (bv)\, dv = \frac{24(6 - b^2) \sin (2\pi b)}{b(36 - b^2)(16 - b^2)(4 - b^2)}$$

$$D_{41} = \int_0^{2\pi} \sin^5 v \cos v \sin (bv)\, dv = -\frac{120 \sin (2\pi b)}{(36 - b^2)(16 - b^2)(4 - b^2)}$$

$$D_{42} = \int_0^{2\pi} \sin^5 v \cos v \cos (bv)\, dv = \frac{120[1 - \cos (2\pi b)]}{(36 - b^2)(16 - b^2)(4 - b^2)}.$$

REFERENCES

1. Bennett, S. B., and Thomas, L. C., The *Telstar* Communications Satellite Experiment Plan, AIEE Trans., No. 63-952, May 6, 1963, pp. 9–10. See also B.S.T.J., **42,** July, 1963, p. 765.
2. Hill, D. W., Calculation of the Spin-Axis Orientation of the *Telstar* Satellites from Optical Data, B.S.T.J., **42,** Nov., 1963, p. 2943.
3. Courtney-Pratt, J. S., Hett, J. H., and McLaughlin, J. W., Optical Meas-

urements on *Telstar* to Determine the Orientation of the Spin Axis and the Spin Rate, Jour. SMPTE, **72,** June, 1963, pp. 462–484.
4. *The American Ephemeris and Nautical Almanac for the Year 1962*, U. S. Government Printing Office, Washington, D. C., 1960, p. 482.
5. Ref. 4, pp. 466–471.
6. Smart, W. M., *Textbook on Spherical Astronomy*, Cambridge Press, 1956, pp. 116–117.
7. Vestline, E. H., et al., Description of the Earth's Main Magnetic Field and Its Secular Change, 1940–1945, Carnegie Institution of Washington, Publication 578, 1947.
8. Vestline, E. H., et al., The Geomagnetic Field, Its Description and Analysis, Carnegie Institution of Washington, Publication 580, 1959.
9. Hrycak, P., et al., The Spacecraft Structure and Thermal Design Considerations, B.S.T.J., **42,** July, 1963, p. 971.
10. Roberson, R. E., and Tatistcheff, D., The Potential Energy of a Small Rigid Body in the Gravitational Field of an Oblate Spheroid, J. Franklin Inst., **262,** 1956, pp. 209–214.
11. Harnwell, G. P., *Principles of Electricity and Electromagnetism*, 1st ed., McGraw-Hill, 1938, p. 377. For precessional theory similar to that of Section 4.6, but for circular orbits only, see: Bandeen, W. R., and Manger, W. P., Angular Motion of the Spin Axis of the *Tiros I* Meteorological Satellite Due to Magnetic and Gravitational Torques, NASA TN D-571, April, 1961.
12. Allen, C. W., *Astrophysical Quantities*, Athlone Press, 1955.
13. See Ref. 6, pp. 107–108.
14. See Ref. 6, p. 111–113.
15. Danby, J. M. A., *Fundamentals of Celestial Mechanics*, Macmillan, New York, 1962, pp. 128–129.
16. Goldstein, H., *Classical Mechanics*, Addison-Wesley, 1959.
17. Yu, E. Y., Spin Decay, Spin-Precession Damping, and Spin-Axis Drift of the *Telstar* Satellite, B.S.T.J., **42,** Sept., 1963, p. 2169.
18. Jakes, W. C., Participation of the Holmdel Station in the *Telstar* Project, B.S.T.J., **42,** July, 1963, p. 1421.
19. Harris, D. L., *Planets and Satellites*, ed. Kuiper and Middlehurst, Chicago, 1961.
20. Delchamps, T. B., et al., The Spacecraft Test and Evaluation Program, B.S.T.J., **42,** July, 1963, p. 1020 and p. 1024.
21. Phillips, H. B., *Vector Analysis*, John Wiley, 1933.
22. Pierce, B. O., *A Short Table of Integrals*, 4th ed., Ginn, 1957.